FAILURE ANALYSIS IN ADHESIVELY BONDED COMPOSITE JOINTS

A THESIS SUBMITTED TO
THE GRADUATE SCHOOL OF NATURAL AND APPLIED SCIENCES
OF
MIDDLE EAST TECHNICAL UNIVERSITY

BY

REYHAN DENIZ ATAY

IN PARTIAL FULFILLMENT OF THE REQUIREMENTS
FOR
THE DEGREE OF MASTER OF SCIENCE
IN
MECHANICAL ENGINEERING

SEPTEMBER 2019

Approval of the thesis:

FAILURE ANALYSIS IN ADHESIVELY BONDED COMPOSITE JOINTS

submitted by **REYHAN DENİZ ATAY** in partial fulfillment of the requirements for the degree of **Master of Science in Mechanical Engineering Department, Middle East Technical University** by,

Prof. Dr. Halil Kalıpçılar
Dean, Graduate School of **Natural and Applied Sciences** _____

Prof. Dr. M. A. Sahir Arıkan
Head of Department, **Mechanical Engineering** _____

Prof. Dr. Almıla Güvenç Yazıcıoğlu
Supervisor, **Mechanical Engineering, METU** _____

Prof. Dr. Kemal Levend Parnas
Co-Supervisor, **Mechanical Engineering, TEDU** _____

Examining Committee Members:

Assoc. Prof. Dr. Gökhan Özgen
Mechanical Engineering, METU _____

Prof. Dr. Almıla Güvenç Yazıcıoğlu
Mechanical Engineering, METU _____

Prof. Dr. Kemal Levend Parnas
Mechanical Engineering, TEDU _____

Assoc. Prof. Dr. Demirkan Çöker
Aerospace Engineering, METU _____

Assist. Prof. Dr. Şehram Dizeci
Mechanical Engineering, TEDU _____

Date: 09.09.2019

I hereby declare that all information in this document has been obtained and presented in accordance with academic rules and ethical conduct. I also declare that, as required by these rules and conduct, I have fully cited and referenced all material and results that are not original to this work.

Name, Surname: Reyhan Deniz Atay

Signature:

ABSTRACT

FAILURE ANALYSIS IN ADHESIVELY BONDED COMPOSITE JOINTS

Atay, Reyhan Deniz
Master of Science, Mechanical Engineering
Supervisor: Prof. Dr. Almıla Güvenç Yazıcıoğlu
Co-Supervisor: Prof. Dr. Kemal Levend Parnas

September 2019, 89 pages

In this thesis study, the mechanical performance and failure behavior of adhesively bonded structures are investigated. A mechanical test program is conducted on single lap shear specimens. Without changing composite and adhesive base materials, parameters including the stacking sequence, adherend thickness and bond line length are considered. Additionally, an analytical model is created and implemented into a finite element analysis program, to perform failure analysis and to determine the load carrying capacity of the selected composite part in an airplane wing structure. For modelling the bond line, the cohesive zone approach is used. Both damage initiation and propagation are performed with the same approach. The effect of geometry on the mechanical performance of the adhesively bonded joints are analyzed. Analytical results are used to determine the stress concentrations within the joint to understand the failure mechanisms.

Keywords: Adhesive Bonding, Single Lap Joint, Finite Element Model, Composite Structures, Cohesive Zone Model

ÖZ

KOMPOZİT YAPIŞTIRMA BAĞLANTILARININ HASAR ANALIZI

Atay, Reyhan Deniz
Yüksek Lisans, Makina Mühendisliği
Tez Danışmanı: Prof. Dr. Almıla Güvenç Yazıcıoğlu
Ortak Tez Danışmanı: Prof. Dr. Kemal Levend Parnas

Eylül 2019, 89 sayfa

Bu tezde, yapıştırıcı ile bağlanmış yapıların mekanik performansı ve hasar davranışları incelenmiştir. Bindirme bağlantı numuneleri üzerinde öncelikle bir mekanik test programı icra edilmiştir. Kompozit ve yapıştırıcı malzemeler değiştirilmeden, serilim, yapışan malzemelerin kalınlığı, yapıştırma yüzey uzunluğunu içeren parametrelerin etkileri değerlendirilmiştir. Yapıştırma bağlantılarda geometrinin mekanik performansa etkisi incelenmiştir. Bunlara ek olarak, uçak kanat yapısının seçilmiş kompozit parçasının hasar analizini yapmak ve yük taşıma kapasitesini belirlemek için bir analitik model oluşturulmuş ve bu model sonlu eleman analiz programı yardımıyla incelenmiştir. Yapıştırıcı hattının modellenmesi için yapışkan yüzey (cohesive zone) yaklaşımı kullanılmıştır. Hasar başlangıcı ve ilerlemesi aynı yaklaşımla incelenmiştir. Analitik sonuçlar, kırılma mekanizmasını belirlemek amacıyla gerilme yığılmalarını belirlemekte kullanılmıştır.

Anahtar Kelimeler: Yapıştırma Bağlantıları, Bindirme Bağlantıları, Sonlu Elemanlar Analizi, Kompozit Yapılar, Kohesif Alan Yaklaşımı

To my Family

ACKNOWLEDGEMENTS

I would like to express my deepest gratitude to my supervisors Dr. Almıla Güvenç Yazıcıoğlu and Dr. Levend Parnas for their support and patience.

I would like to first dedicate my sincere appreciation to my co-supervisor Levend Parnas for providing me the chance and enlightening my problems through the research.

I feel very fortunate and honorable to work with Saeid Hosseinpour Dashatan during my thesis. I want to thank him for his endless support, enlightenment and contribution to this thesis.

My experiments were partially supported by Rüzgem Structures and Materials Laboratories. The support and help of Dr. Demirkan Çöker, Miraç Onur Bozkurt and Emine Burçin Özenç are particularly appreciated.

This thesis study is conducted with the support of Turkish Aerospace. This support is highly appreciated for performing experiments. Furthermore I want to thank my colleagues in Turkish Aerospace for helping me on every moment that I got into problems.

Last but not the least, I would like to thank my husband, family and friends for supporting and encouraging me all the way coming along.

TABLE OF CONTENTS

LIST OF TABLES

TABLES

LIST OF FIGURES

FIGURES

LIST OF ABBREVIATIONS

ABBREVIATIONS

2D	Two-Dimensional
3D	Three-Dimensional
ASTM	American Society for Testing and Materials
B-K	Benzeggagh- Kenane
CZM	Cohesive Zone Model
DCB	Double Cantilever Beam
ENF	End-Notch Flexure
FRP	Fiber Reinforced Plastics
FE	Finite Element
FEA	Finite Element Analysis
LEFM	Linear Elastic Fracture Mechanics
MAXS	Maximum Nominal Stress Criterion
QUADS	Quadratic Nominal Stress Criterion
SLJ	Single Lap Joint
UD	Uni-Directional
VCCT	Virtual Crack Closure Technique
XFEM	Extended Finite Element Modelling

LIST OF SYMBOLS

SYMBOLS

E_1	Longitudinal modulus
E_2	Transverse modulus
E_3	Transverse-thickness modulus
G_{12}	In-plane shear modulus
G_{13}, G_{23}	Interlaminar shear moduli
G_I	Fracture energy under Mode I
G_{II}	Fracture energy under Mode II
G_{III}	Fracture energy under Mode III
G_c	Fracture toughness
K_{nn}	Penalty Stiffness in Normal Direction
K_{ns}, K_{ss}	Penalty Stiffness in Shear Direction
K_{COH}	Penalty Stiffness Matrix
k	Bending moment factor
L	Length
M	Bending moment
Nu_{12}	In-plane Poisson's ratio
P	Load
P_s	Adherend Yield Load

t	Thickness
t_n	Normal Contact Stress in the Pure Normal Mode
t_s	Shear Contact Stress Along the First Shear Direction
t_t	Shear Contact Stress Along the Second Shear Direction
w	Width
η	B-K Parameter
δ	Displacement
δ_n	Displacement in Normal Direction
δ_s	Displacement in Shear Direction
σ_s	Peel Stress
σ_y	Yield Strength
α, β, γ	Exponents
$\langle\,\rangle$	MacAuley bracket

CHAPTER 1

INTRODUCTION

Adhesive bonding is a joining process in which two neighboring surfaces are connected with the application of a bonding agent. Due to its considerable advantages, adhesive bonding is a frequently used method in the aerospace industry; especially for joining laminated composite structures [1].

The conventional mechanical fastening results in stress concentrations around the fasteners and fiber breakage during the implementation in laminated composites. With the use of adhesive bonding, the drawbacks of the mechanical fastening can be decreased and structural integrity can be increased. In addition, lightweight structures can be obtained with adhesive bonding [1].

In spite of the advantages of adhesive bonding, material models and failure criteria are not well developed in contrast to mechanical fastening. For that reason, "overdesigned" structures with a high factor of safety are generally obtained to ensure safety considerations which leads to creation of expensive and redundantly heavier designs. Therefore, improving the adhesive methodologies may help to utilize adhesive bonding joints more efficiently [2].

Depending on the application, three different methods are used to perform a bonding in a joint. These methods are; co-curing, co-bonding and secondary bonding. Although secondary bonding method provides stronger joints for complex-shaped structures, co-curing and co-bonding are preferred due to their shorter curing cycles [3]. Bonding method has a crucial effect on failure modes and joint strength. Therefore, the most appropriate method should be chosen to meet the requirements [3].

Single lap joint (SLJ) is one of the simplest form of the adhesively bonded joints which is considerably used in structural joints. SLJ is preferred due to ease in preparation,

capability of using substrates with different materials and thicknesses. In addition, a combination of uniaxial and shear loading can be investigated with this simple joint model as shown in Figure 1.1.

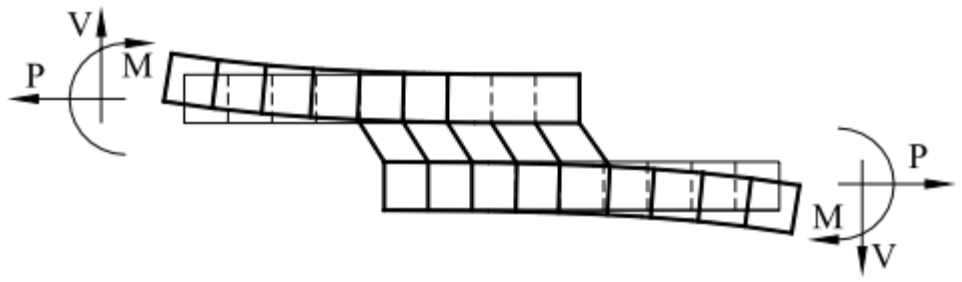

Figure 1.1. A Simple Single Lap Joint Representation *[8]*

Mechanical properties of adhesively bonded joints are obtained by using standard test procedures. For joints under the shear loading, there are several ASTM (American Society for Testing and Materials) standards. ASTM 1002, ASTM D 3165, ASTM D 5656 which are commonly used ones to measure apparent shear strength and apparent shear stress-strain relation of adhesives. The results can be used in the specification of adhesive and geometry of bonded joints [4]

In adhesive bonded joints, three different failure modes would take place which are cohesive failure, adhesive failure and adherend failure. Loading conditions, improper surface preparation, curing process are the most important factors which affect the failure modes. Understanding the mechanism of these failure modes is crucial in design and analysis of bonded joints [5].

Joint strength can be determined using stress distribution and suitable failure criteria. The stress distribution of a bonded joint can be obtained by either a closed-form model or finite element analysis. Finite element analysis generally preferred over closed-form solutions due to ease of calculation, saving time and design effort.

There are three main methods to perform failure analysis in bonded joints, which are continuum mechanics, fracture mechanics and damage mechanics. Within these methods, continuum mechanics have difficulty to give a solution at singularities and fracture mechanics requires a pre-existing crack. Among these restrictions, damage mechanics has an ability to predict both damage initiation and propagation with a specific method which is Cohesive Zone Modeling (CZM) [6]. Through cohesive zone modeling, stress and damage analyses are performed within the same design tool. In this approach, joint strength is determined by using stress distribution and suitable criteria for damage initiation and propagation. In the finite element modeling, it can be assumed that negative effects arise from manufacturing faults are negligible [4][7].

1.1. Motivation of Thesis Study

Adhesive bonding has been used extensively in the aerospace industry. One of the most frequently encountered bonded joint types in aerospace structural applications is the single lap joint in which failure mechanisms are important depending on the area of usage. However, they have not been given the necessary emphasis especially for asymmetric composite joints. That is why in this thesis, single lap joints with asymmetric configurations are considered in detail for better understanding of the failure mechanisms in such geometries.

1.2. Objective and Scope of Study

The aim of this study is to investigate the mechanical performance in adhesively bonded single lap joints. In this context, a set of mechanical tests and numerical analyses are performed on composite bonded joints.

In order to determine the influence of the design parameters on joint strength, SLJ tests of specimens with different thickness, composite sequence and overlap length are performed. ASTM 3165 standard procedure is followed in this test campaign.

ABAQUS/CAE (SIMULA™ by Dassault Systèmes®) is used to perform finite element analyses. The interface of adhesive and adherend is modeled using cohesive

zone approach. Finite element analysis results are used to understand the failure modes of single lap joints.

Chapter 2 is devoted to the detailed information of adhesively bonded joints in composite structures to support the background of the study. A piece of brief information about the advantages of adhesive bonding is given. Afterward, joint selection and failure modes of single lap joints are discussed. In addition, failure mechanisms of bonded joints are mentioned in the scope of this chapter.

In Chapter 3, CZM method, the theory behind this modelling technique and analytical formulations are represented.

The mechanical test method and modelling methodology of single lap joints are given in Chapter 4. Detailed information about test specimens, specimen configurations and test method given in this chapter. Later finite element model represented with element types, modelling approach, boundary conditions and applied failure modes.

In Chapter 5, SLJ test results are investigated in detail. Microscopic examination on test specimens and observation of crack initiation and propagation with high-speed camera test are included in this chapter. Effects of the stiffness of the adherends, thickness-to-joint length ratio of the SLJ are examined. Stress distributions and failure modes are indicated in finite element analysis.

Finally, Chapter 6, comprises of the summary of this thesis study.

1.3. Literature Survey

This section starts with a background of adhesive bonding and bonded lap joints. Analytical approaches in general examine the strength behavior of adhesively bonded joints. Specifically, single lap joint studies are investigated in more detail. Publications examining failure modes of adhesively bonded structures have been comprehensively studied. And here the results of a detailed survey on the cohesive zone model are presented.

Many studies have been performed on adhesively bonded joints with the use of steel material for adherends, however, studies considering composite joints with asymmetric single lap joints are quite rare in literature.

In one of the early works, Volkersen [8] created a simple analytical solution for adhesively bonded single lap joints in 1938. In this closed-form solution, it was assumed that the adherends are effected by only tensile forces while the adhesive deformation is due to only shear force. Moreover, bending effects that are arisen by the eccentricity of the adherents are not taken into account. Different from Volkersen, Goland and Reissner [8] considered bending effects of single lap joints. However, their analytical solution adhesive thickness is not considered and an infinitely thin adhesive layer is assumed. Hart-Smith originated the solution of Goland and Reissner and the closed form solution improved by taking into account of adhesive layer thickness [8].

Later, Tsai and Morton [18] reviewed theoretical solutions on single lap joints including Goland and Reissner's study [44]. Tsai and Morton focus on the stress singularity that takes place at the corners of the bonded single lap joints which is not taken into account in [44]. They indicated that the highest stress appears at interface corners between adherend and adhesive which may initiate failure at that point.

Davis and Bond [9] investigated the failure mechanism of bonded joints by focusing on the characterization of failure modes. According to the study, adherend failure is the most desirable failure mode, since it shows that a proper adhesion is obtained at the interface and the adhesive load caring capacity is higher than the surrounding structure. However, due to the faults in production processes, cohesive and adhesive failure modes are more prevalent in real life applications. Identifying the failure mode can be used for an effective design and production method.

Karachalios et al. [10] performed experimental and finite element analysis on the single lap joints with steel adherends. The joint strength of SLJs were investigated by changing the adherend thickness, adhesive thickness and overlap length. They

conclude that the overlap length doesn't have an important effect on the joint strength. On the other hand, the thickness of the adherends effect the joint strength significantly. According to the comparisons of experimental results with a finite element model, they observed that the crack initiated at the ends of the overlap due to local strains created by tension loads. Decreasing the adherend thickness leads to higher peel stress at the tension side of the overlap edge. Therefore, joints with thicker adherends are concluded to be stronger.

Kupski et al. [11] studied the effects of composite stacking on the failure behavior of bonded lap joints. Composites adherends with four different stacking sequence were used in this study. According to the tests and analyses, they observed that the increase in bending stiffness of the adherends increases the load at damage initiation and results in damage initiation on the bond line. Also, they considered interface ply effects on failure mode in adhesively bonded joints using 0º and 90 º plies at the interface. They conclude that using 0º plies causes adhesive failure, while 90º plies causes failure inside the adherend.

In the paper by Kutscha and Hofer [12], a parametric study is performed and rather general conclusions are arrived. It is concluded that the joint strength and fatigue strength highly depend on the modulus of adhesive. Higher strength is obtained with the plastic adhesive of lower modulus than the brittle and stiff adhesives. They also concluded that joint strength depends on the length-to-thickness ratio where joint strength decreases with an increase in overlap ratio (L/t).

Also, Kutscha and Hofer [12] investigated symmetric and asymmetric single lap joints. In asymmetric joints, the crack initiation is observed at the end of thinner adherend because of maximum shear stress developing in that area. In joints with symmetric adherends, crack initiates in both ends simultaneously due to the symmetry of the joint.

Asymmetric single lap joints also analyzed by Hart-Smith in 1985 [13]. In their paper, they show that, for symmetric joints, the same peel stress concentration is formed in

both ends of the overlap. On contrary, using adherends with different thicknesses leads to an increase in bending moment and peel stress at the end of the thinner adherend. The conclusion is made in the paper as the increase in the imbalance between the adherends, decreases the bending strength of the joint.

Another study on different adherends is performed by Reis et al. [14] who aimed to compare shear strength of various SLJs which have adherends with different stiffnesses. It is performed on adherends using composite, steel and aluminum alloy. It is concluded that with the increase in rigidity of the joint, rotation of the joint decreases which produces a uniform stress distribution within the adhesive. A distinct conclusion is captured in Reis's paper as they indicate that the strength of the joint is determined by the less stiff material.

The cohesive model concept is first introduced by Dugdale [15] where a non-linear zone is observed in front of the crack tip. This zone can be named as cohesive zone and the forces resisting the crack opening are cohesive forces.

Modeling with cohesive elements exhibits some convergence problems during crack growth analyses. Many researchers have faced such problems and developed various guidelines to select the stiffness of the cohesive elements. Among these studies, Camanho [16] and Zou et al. [17] recommended a quite higher value than the nominal stiffness of the material. However Turon [18] generated solutions including the simulation of progressive delamination by considering the stiffness of CZM and length of the cohesive zone. He proposed an interface stiffness relation for increasing stiffness value of the cohesive elements to overcome the numerical problems. In addition, he worked on the calculation of the cohesive zone length. It is observed from the studies that, decrease in interfacial strength improves the convergence of the solution. Reduction of interfacial strength results in an increase in the cohesive zone length and in order to obtain accurate results, the minimum number of elements must be defined in the cohesive zone span.

Cohesive layers are widely simulated with zero thickness elements. Alfano and Crisfield (2001) [19] worked on a model where the thickness of the interface elements are relatively very thin compared with the overall geometry considered. The interface is modeled with zero-thickness elements to obtain an effective finite element discretization. As the model loaded, zero thickness elements gain a finite thickness due to relative displacement of the nodes until the complete failure [19].

There are two ways to establish CZM in a bonded joint in the literature. One of the CZM concepts is based on the replacement of the adhesive bulk material with a single row of cohesive elements along the bond, while the second concept uses zero thickness cohesive elements for the interface between adhesive and adherend which simulates the adhesive failure in bonded joints. With the modeling of adhesive bulk material with single layer cohesive elements, thickness wise effects and stress concentrations can not be calculated[6]. For that reason, the more versatile model has been selected by many studies in which cohesive interface elements are used to simulate interface crack in bonded joints. Tvergaard and Hutchinson [41], Pardoen et al. [15], Kafkalidis et al. [16] are the researchers who used cohesive elements and the tie constraint approach for the interface between the adherend and adhesive material which allows finer discretization to simulate a more accurate interface crack behavior.

In this study, the failure behavior of adhesively bonded single lap joints with composite adherends are investigated on the contrary to the literature where mostly joints with steel adherends are studied. Besides, unbalanced single lap joints are underline of this study which are quite rare in the literature. Mechanical tests and finite element analyses are performed to determine the crack initiation and propagation behavior on unbalanced bonded lap joints. Effect of stacking sequence, adherend thickness and bond line are investigated on the mechanical performance of the adhesive bonded joints are analyzed.

CHAPTER 2

ADHESIVELY BONDED JOINTS IN COMPOSITE MATERIALS

Bonded joint applications have been performed in various industries due to their considerable advantages. Especially, for lightweight structures have been obtained with such bonding methods where adhesive bonded joint usage decreased weight significantly in the aerospace industry.

Despite mechanical fastening has various adverse effects on the structure, there are quite a number of studies performed so far and thus the failure behavior in mechanical fastening can be estimated more accurately. However, the analyses for bonded joint behavior and material models are not yet mature as the mechanical fastening. Therefore, due to safety considerations, there is a tendency for ‘overdesign’ for composite structures with bonded joints. Improvements on design and methodology can increase the efficiency of the adhesively bonded structures [6].

The use of fiber-reinforced materials have increased significantly in recent years for known reasons. Conventional mechanical fastening methods are known to result in fiber damages in composite structures and cause premature crack initiations. By using adhesive bonding, such problems are mostly averted, continuous load paths are obtained and even lightweight structures can be modelled. A summary of advantages and disadvantages for adhesive and mechanical bondings are given in Table 2.1.

It can be concluded that adhesive bonding is highly desirable in fiber-reinforced structures due to its numerous advantages.

Table 2.1. *Advantages and Disadvantages of Mechanical Fastening and Adhesive Bonding*

	Advantages	Disadvantages
Mechanical Fastening	• No need for surface preparation • Ease of disassemble and reassemble	• Stress concentration around fasteners • Increases the structure weight
Adhesive Bonding	• High strength to weight ratio • Uniform stress distribution • Higher damage tolerance • Reduces fabrications cost • Provides design flexibility	• Special surface preparation necessary • Non-destructive test necessary • Permanent assembly • Increase fabrication time due curing time • Lower resistance to high temperature • Consideration needed for temperature and humidity. • Safety and environmental consideration

2.1. Adhesive Bonding of Composites

Adhesive bonding are commonly performed by three methods, co-curing, co-bonding and secondary bonding. Bonding method has a vital effect on failure modes and joint strength. Therefore, the most appropriate method should be chosen according to need.

2.1.1. Co-Curing

Co-curing process as shown in Figure 2.1 achieved by curing two uncured substrate simultaneously with an adhesive which is compatible with the matrix resin. In this process, both substrate and adhesive are cured together with the same operation [23].

Figure 2.1. Co-curing process

2.1.2. Co-Bonding

Co-bonding is a process where one fully cured and one un-cured substrate are bonded together by using an adhesive as shown in Figure 2.2. A need arises in co-bonding process, where to perform surface preparation is applied on the initially cured substrate surface in order to provide an appropriate bonding surface in second stage [23].

Figure 2.2. Co-bonding process

2.1.3. Secondary Bonding

In secondary bonding process, two fully cured substrate are bonded together by using an adhesive(Figure 2.3). The adhesive is cured in room temperature or all the substrate and adhesive are cured again with an autoclave or a heat-blanket [23].

Figure 2.3. Secondary bonding process

2.2. Failure Modes

Classification of failure types for FRP joints are well defined in ASTM D5573 [26]. In this paper, considering ASTM D5573 Standard, a general classification is created and failure types are collected in 3 main groups which are explained in more detail in the following sections.

2.2.1. Cohesive Failure

The cohesive failure represents the failure within the adhesive bulk material (Figure 2.4) which is the most desirable mode of failure. It takes place where peel stress or out of plane stress increases. As a matter of fact, they cause joint eccentricity and large deformations in adherends. The joint eccentricity causes cohesive failure because adhesives are known to be weak in the out of plane direction [27].

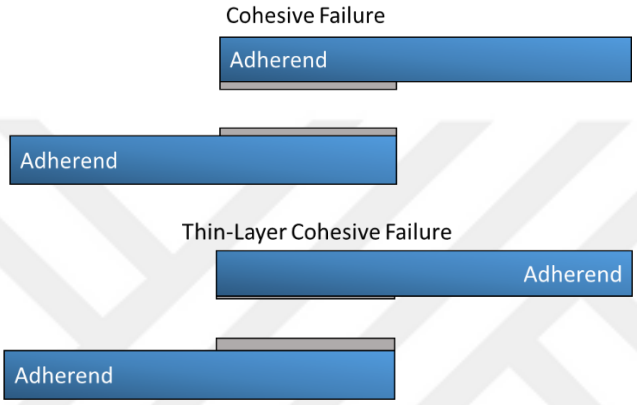

Figure 2.4. Cohesive Failure of Bonded Lap Joint

2.2.2. Adhesive Failure

Adhesive failure would occur along the interface between the adhesive and adherend as shown in Figure 2.5. General cause of this phenomenon is improper surface preparation.

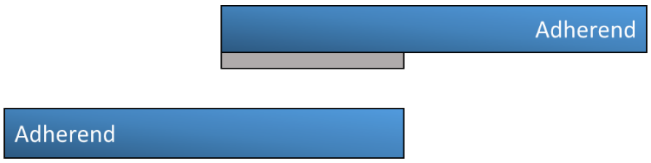

Figure 2.5. Adhesive Failure of Bonded Lap Joint

2.2.3. Adherend Failure

Failure within the FRP substrate is called as adherend failure. Adherend failure either occur with rupturing a piece of FRP substrate or rupture one of the adherend completely. The general cause of failure in adherends are high shear stresses at bonded joints since shear strengths of adhesives are relatively higher than laminates. Adherend failure representation is given in Figure 2.6.

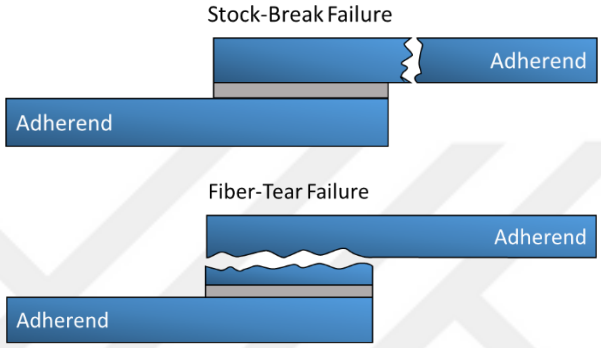

Figure 2.6. Adherend Failure of Bonded Lap Joint

2.3. Failure Analysis of Bonded Joints

Reliable and efficient use of bonded joints is depending on the design and methodology can be costly. Finite element analysis plays an important role at this point to obtain optimum design of structures. By using finite element method, accurate predictions can be achieved for joint strength and failure behavior. There are mainly three approaches to perform failure analyses, which are continuum mechanics, fracture mechanics and damage mechanics.

2.3.1. Continuum Mechanics

General concept in this approach is simply comparing the material allowable with the maximum stress and/or strain values as output of analyses. In continuum mechanics, materials are assumed to be continuous and there is no solution at the singularity

points. Therefore, mesh refinement near the singularity points are highly determinative on the results of the analyses [6].

2.3.2. Fracture Mechanics

In contrast to continuum mechanics, this approach is capable to derive a solution at crack tips. However, a pre-existing crack is required to be defined within this method. While crack initiation can be calculated with continuum mechanics, fracture mechanics is a favorable method to deal with crack propagation.

Fracture mechanics uses the stress intensity factor (K) to determine the stress state at singularity points like a crack tip [34]. Failure mechanism works when the stress intensity factor reaches the fracture toughness of the material. Fracture toughness represents the critical fracture energy (G_c).

Fracture mechanics principle differs depending on the loading on the crack tip as shown in Figure 2.7. There are three mode of loading;

- Mode I; opening mode
- Mode II; in-plane shear mode
- Mode III; out-of-plane shear mode

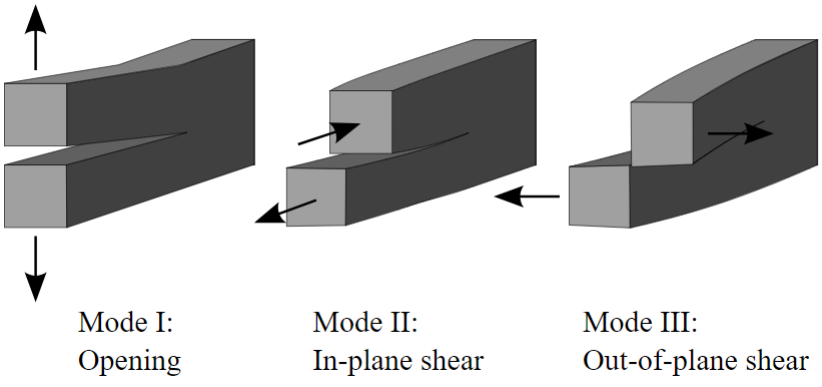

Figure 2.7. Adherend Failure of Bonded Lap Joint

Adhesive lap joints involve mixed mode loading due to the incorporation with different materials and complex stress system [33]. For mixed mode loading, failure criteria is assumed as;

$$\left(\frac{G_I}{G_{Ic}}\right)^{\alpha} + \left(\frac{G_{II}}{G_{IIc}}\right)^{\beta} + \left(\frac{G_{III}}{G_{IIIc}}\right)^{\gamma} = 1 \quad (1)$$

In Equation 1, G_I, G_{II} and G_{III} represent fracture energies under Mode I, Mode II and Mode III respectively. G_{Ic}, G_{IIc} and G_{IIIc} are critical energy values. α, β and γ are exponents and can be taken as $\alpha = \beta = \gamma = 1$ for linear criteria, $\alpha = \beta = \gamma = 2$ for the quadratic criteria.

2.3.3. Damage Mechanics

Damage mechanics is a method to predict both initiation and propagation in the structure until the complete structural failure. It can be divided into two main parts, which are local approach and continuum approach.

The local approach is used to predict the interfacial failure between two surfaces. Interface elements are modelled with zero volume line. While continuum approach uses finite thickness elements to simulate failure of the bulk material (adhesive).

Between these two approaches a specified model is categorized that is called as the cohesive zone model (CZM). CZM is used for the paths defined in local and continuum approaches and combine the response of traction-separation to simulate crack initiation and propagation. In the following chapter, a detailed information and methodology of cohesive zone model is given.

2.4. Adhesively Bonded Single Lap Joints

Single lap joints are one of the widely used joint configurations owing to the possibility of obtaining complex stress conditions in such simple geometry. Different

materials with various thickness and length can be tested with single lap joints. In addition, both shear and uniaxial stresses can be obtained.

The simplest single lap joint configuration is given in Figure 2.8(a). Tensile loading of this configuration generates bending on adherends as a result of joint eccentricity. The geometry faces with peel stresses at the edge of adherends due to bending. To overcome the eccentricity in the joint, and decrease bending effects at overlap edge, doublers are used as shown in Figure 2.8 (c).

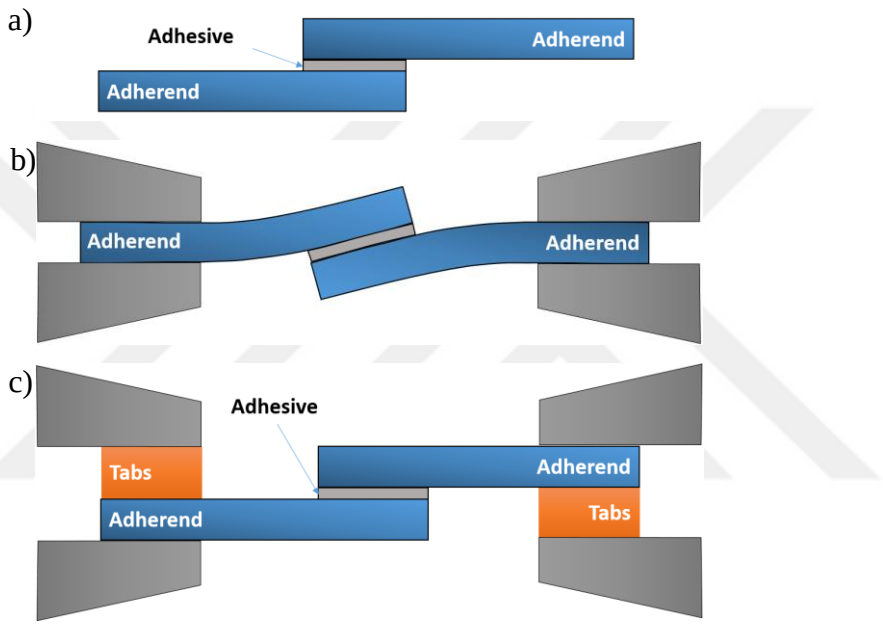

Figure 2.8. Bending behavior of the single lap joints

Single lap joint analyses have been performed for decades to obtain material properties of adhesives and bonded joints. These analyses result in determining stress distributions in adhesives and adherends. The earliest studies on analysis of SLJ performed by Volkersen in 1938 [8] in which it was assumed that the adhesive layer deforms in shear. However, the shear effect on adherends is generally ignored. In other words, bending effect due to eccentric loading is not taken into account. However, by using this simple method, shear stress effect on adhesive of single lap joints can be observed as shown in Figure 2.9 [11].

According to Volkersen model, by representing width of the model with w, overlap length with *l* and applied load with *P*, the shear stress τ can be found as;

$$\tau = \frac{P}{wl} \tag{2}$$

Where the adherend tensile stress assumed to be zero throughout the overlap.

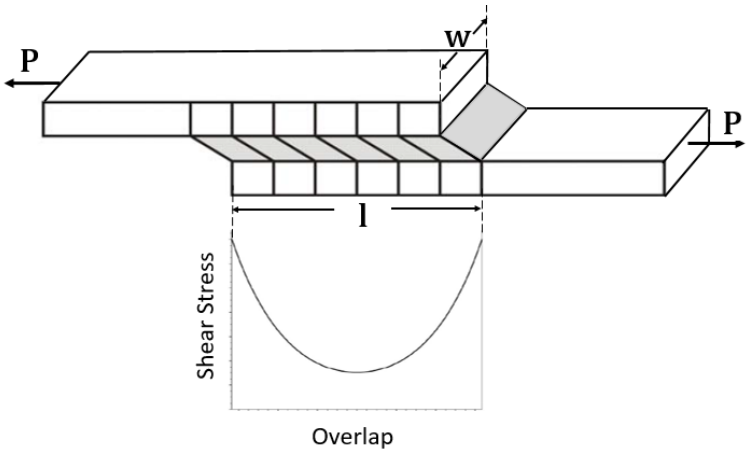

Figure 2.9. SLJ assumption of Volkersen*[8]*

Later, Goland and Reissner [8] developed a modified version of Volkersen model by adding bending effects in their analysis. Bending moment causes a transverse normal stress through the thickness of the adhesive which is called 'peel stress'. Goland and Reissner stress distributions on the overlap is shown in
Figure 2.10. According to the analysis, high stress concentration observed at the edges. Stress concentration decrease towards to center of the overlap.

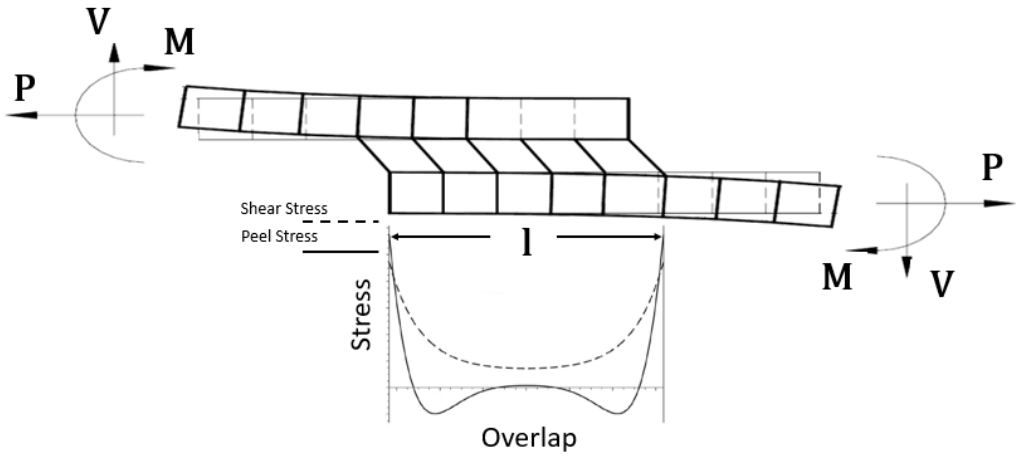

Figure 2.10. SLJ assumption of Goland and Reissner *[8]*

The stress on the overlap σ_s arises due to bending moment M;

$$\sigma_s = \frac{6M}{wt^2} \tag{3}$$

Where *w* is the width and *t* is the thickness of the adhesive and moment calculated as follows;

$$M = \frac{kPt}{2} \tag{4}$$

k variable is bending moment factor defined by Goland and Reissner. This factor taken as 1 approximately for low loads and short overlaps. Where the overlap length is 20 times larger than the thickness of the adhesive, *k* value is taken as zero.

Load for the adherends experiencing both axial and bending stresses calculated as;

$$P_s = \frac{\sigma_y wt}{(1+3k)} \tag{5}$$

where σ_y is the yield strength of the adherend.

Different than Volkersen, Gooland and Reissner model, studies showed that, the maximum shear stress is observed near the ends of the SLJ. However, due to the free surfaces, shear stress goes to zero at the ends. The shear stress distribution shown in Figure 2.11 [24].

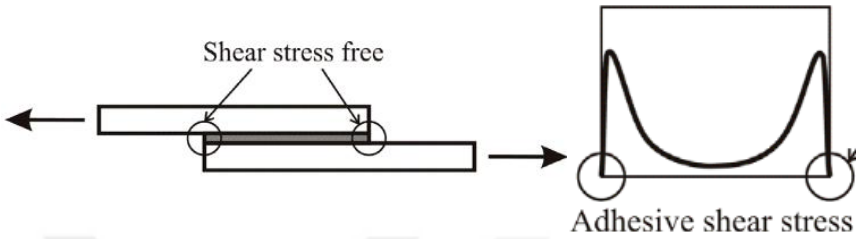

Figure 2.11. Shear stress distribution of adhesive in SLJ *[8]*

High peel stresses are experienced in bonded single lap joints at the end of the overlap. As can be seen in

Figure 2.10, peel stresses are concentrated at overlap edges and a catastrophic decrease is observed at the remaining overlap.

Yang et. al. [25] studied symmetry and asymmetry of single lap joints due to the coupling of axial and transverse forces caused by bending moment. Bending behavior of top and bottom adherends are examined in detail. For symmetric joints as shown in Figure 2.12 both adherend have zero bending moment at its free edge as the reasons explained before, while it reaches to its maximum at the opposing edge. Asymmetric joints, shows same bending moment on the overlap edges with the symmetric joints while higher bending moment observed for rest of the overlap as shown in Figure 2.13.

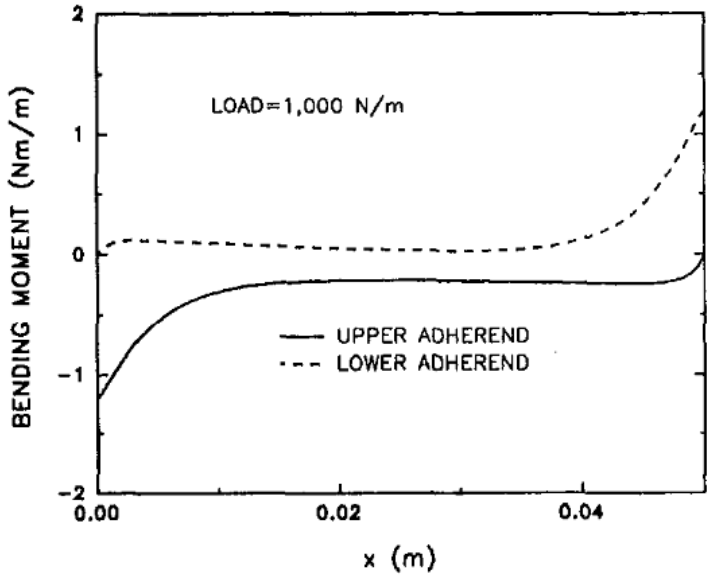

Figure 2.12. Bending moment distribution of symmetric SLJ through the overlap *[25]*

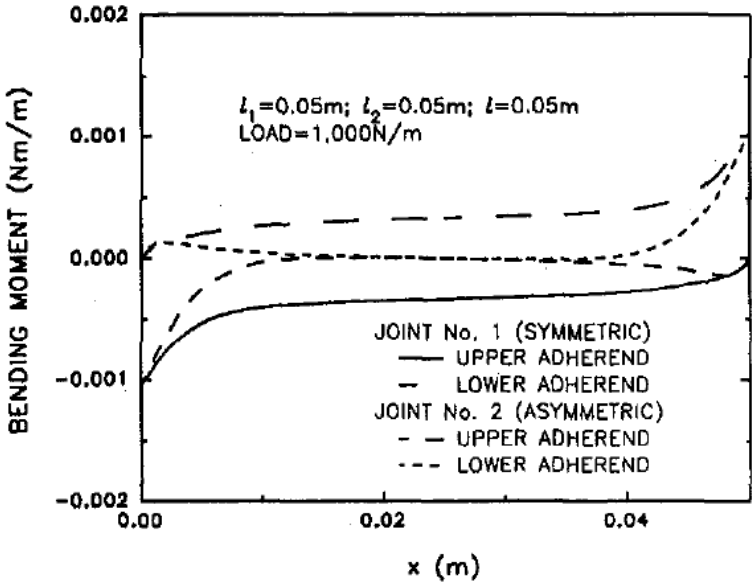

Figure 2.13. Bending moment distribution of asymmetric SLJ through the overlap *[25]*

Also Yang et al. showed the axial stress distribution on upper and lower adherends through the overlap in Figure 2.14. It can be seen that, on the right edge of upper adherend, the maximum stress state is reached while lower adherend has no stress on its edge. On the left edge, an opposite behavior can be observed. Applied load always equals to the summation of total axial stresses at each cross-section.

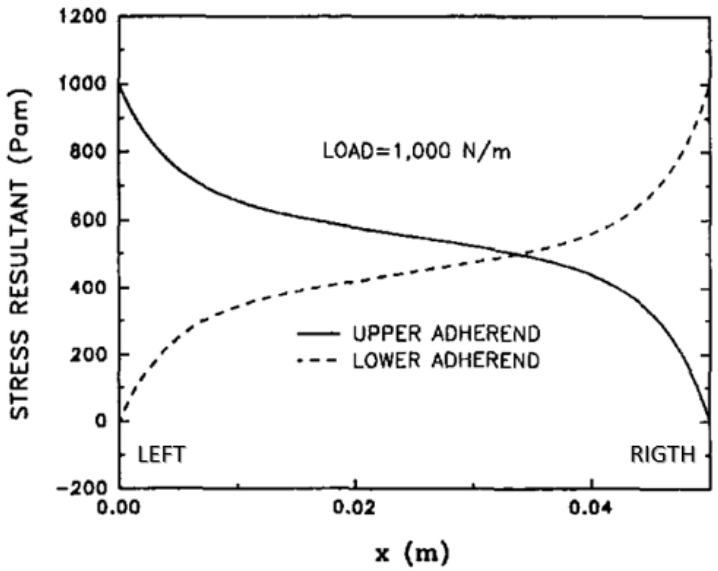

Figure 2.14. Axial stress resultant of single lap joint adherends through the overlap *[25]*

The single lap joints with identical adherends face equal peel stress at the ends of overlap. At that situation cracks initiates from both ends. However, when stiffness of adherends are different than each other, the adherend which has lower bending stiffness, faces with higher peel stress at its end. Therefore, crack initiation is expected at the end of adherend with lower stiffness [13].

2.4.1. Standard Test Procedure for Single Lap Joints

Characterization of the adhesive properties is useful for reliable design and analysis of bonded lap joints. With the use of suitable standard test procedure, reliable data on the mechanical properties can be obtained.

ASTM D 1002 – "Standard Test Method for Apparent Shear Strength of Single-Lap-Joint Adhesively Bonded Metal Specimens by Tension Loading (Metal-to-Metal)" [28] is one of the recommended standard test procedure used to predict the apparent shear strength. This procedure then replaced with ASTM D3165 - "Strength Properties of Adhesives in Shear by Tension Loading of Single-Lap-Joint Laminated Assemblies" [29] which overcomes the joint eccentricity with the addition of two

doubler into SLJ geometry. In both of these standards, thin metallic adherends are recommended to be used however it is indicated that, by considering thickness and rigidity of the adherends plastic adherends can also be use.

One of the other most common test procedure in SLJ is ASTM D 5656 – "Standard Test Method for Thick-Adherend Metal Lap-Shear Joints for Determination of the Stress-Strain Behavior of Adhesives in Shear by Tension Loading" [30]. This standard is used to calculate apparent shear stress-strain relation in SLJ with thick adherends. No yielding and small rotation is observed in overlap region. By this way more uniform stress distribution can be obtained in SLJ. The related standard test procedures are represented in Figure 2.15.

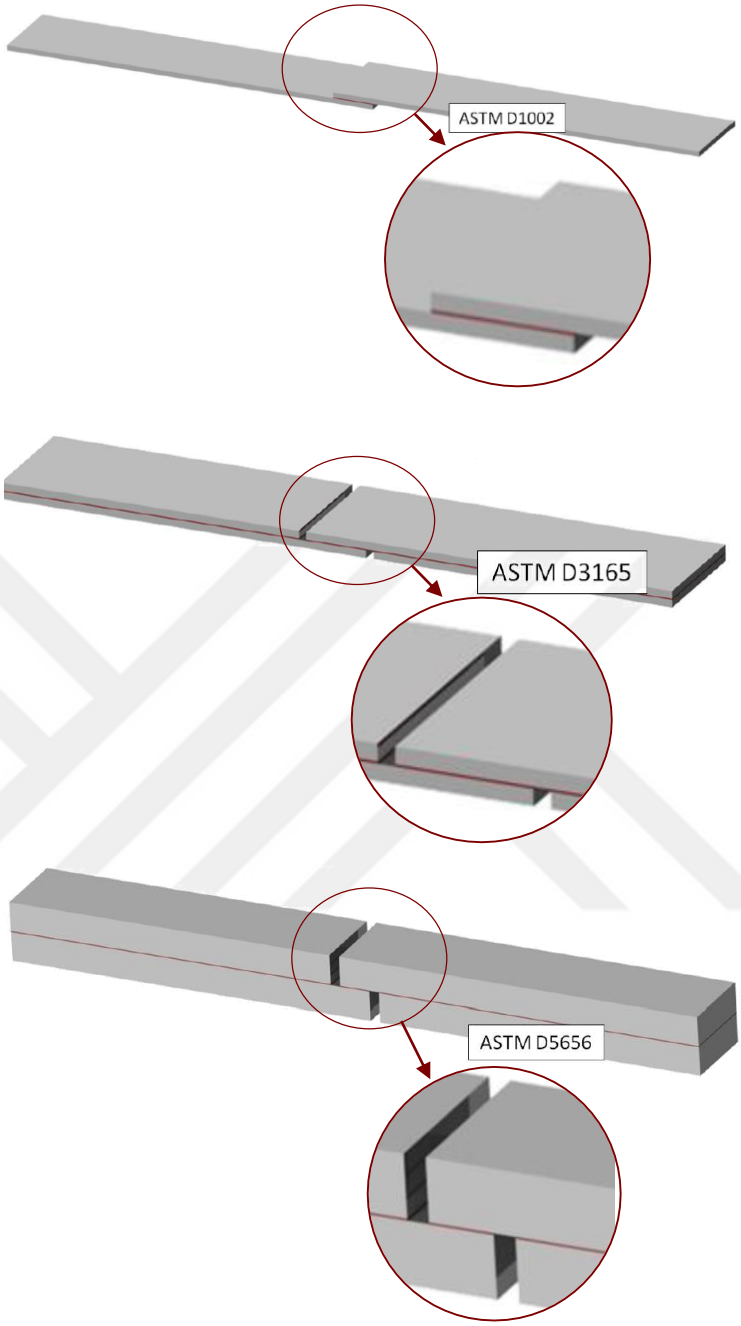

Figure 2.15. Standard SLJ specimens

CHAPTER 3

COHESIVE ZONE MODELLING

Crack extension analyses usually follow procedures of fracture mechanics or damage mechanics. When non-linearities are neglected, LEFM is a viable method to predict the crack propagation behavior of an initially defined crack. A number of techniques are available out there including VCCT, J-integral, and stiffness derivative. These methods are implemented easily in two-dimensional problems since a crack propagates only in one dimension. However, an initial definition of crack location is necessary to implement these methods. Even so, problems may arise when multiple cracks propagate simultaneously. Moreover, the computational effort is dramatically increased in three-dimensional problems. To overcome these problems, new interface models are needed to be developed including the cohesive zone model [19].

The cohesive zone model has been used to simulate damage initiation and propagation in bulk regions or at the interface of adhesively bonded joints. The theory of CZM is based on the elongation of cohesive elements up to an allowable traction value. When traction reaches to a critical value, the crack initiation starts and it propagates until the complete failure. Although the cohesive zone model on the other hand does not require the existence of an initial crack, the maximum traction value to start the crack and the critical energy release rate to complete the failure are required initially. In addition, shape of CZM belonging to the material also defined in the beginning of analysis.

Traction separation law, shown in Figure 3.1, represents the damage initiation and propagation on a simple DCB specimen. The first part of the traction separation law represent the damage initiation phase which ends with the traction value reaches to critical traction. At the start of this zone, the displacement is zero and at the maximum traction the displacement reaches to δ_c. The second part of the traction separation law

represent the damage propagation phase which complete when the area under the traction-separation curve reaches to fracture toughness G_c where also the displacement reaches to maximum displacement δ_f. The relation between cohesive traction T_i and displacement δ_i can be expressed as (where K_i represents the cohesive stiffness)

$$T_i = K_i \delta_i \tag{6}$$

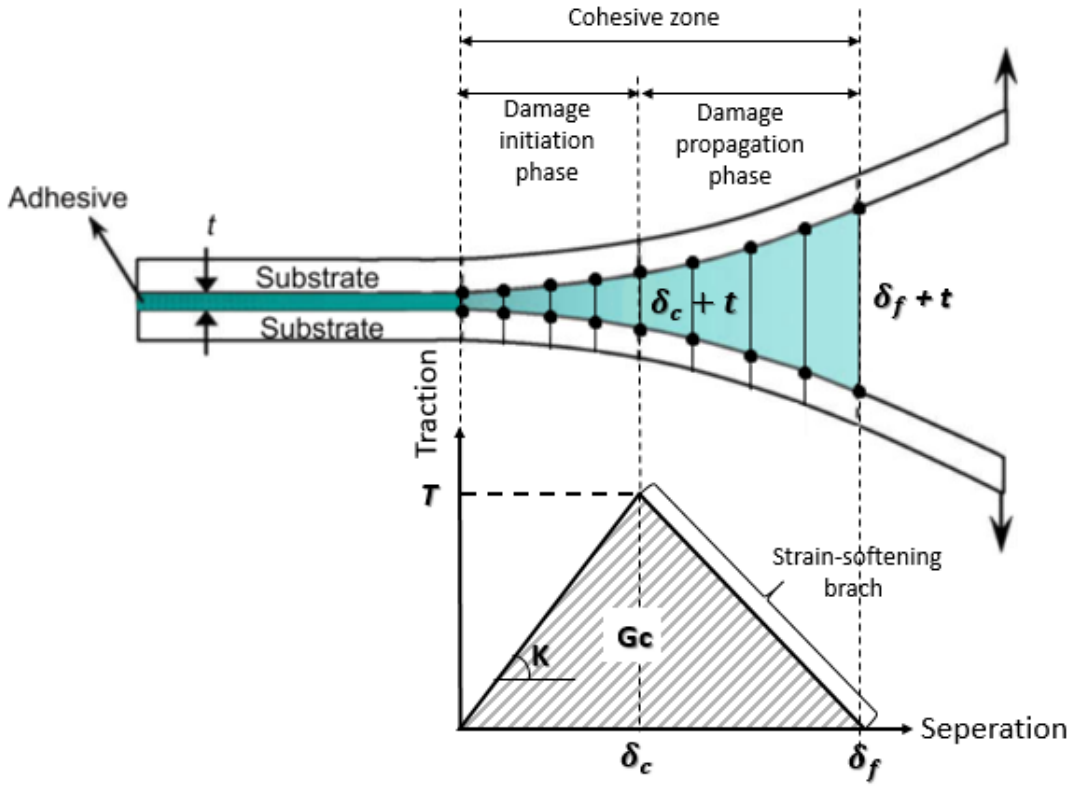

Figure 3.1. Traction-separation law [34]

In Abaqus 2009 documentation [36], it is assumed that 3D cohesive models deflect under three strain component which are through the thickness strain and two transverse shear strains. For 2D problems, one strain through the thickness direction and one transverse shear strain are assumed to be included in the cohesive modelling. For 2D problems, the constitutive law is determined as;

$$T = \begin{Bmatrix} T_n \\ T_s \end{Bmatrix} = \begin{bmatrix} K_{nn} & K_{ns} \\ K_{ns} & K_{ss} \end{bmatrix} \begin{Bmatrix} \delta_n \\ \delta_s \end{Bmatrix} = K_{COH}\,\delta \tag{7}$$

where K_{COH} is the penalty stiffness matrix of the cohesive zone elements. Determining the optimal stiffness value of the cohesive element plays an important role in the numerical analysis due to convergence issues of the model [37]. In a study by Camanho et al.[16], it is stated that a high initial stiffness value retains top and bottom elements in linear elastic zone while elements under the loading to failure. However Yang and Cox stated in their paper that redundantly high stiffness may require extremely fine meshes to overcome the formation of traction oscillations [38].

Various initial stiffness value assumptions has been made in the literature. Among these studies, Camanho [16] defined a penalty stiffness value as 10^6 N/mm^3 for composite laminates, while Zou et al. [17] recommended $10^4 – 10^7$ times higher value for interlaminar shear and tensile strength as interface stiffness per length.

Damage initiation

Under pure mode (Mode I, Mode II, or Mode III), crack initiates at the point where interfacial strength reaches to a critical value (T_n^c, T_s^c, T_t^c)

$$T_i = T_i^c \tag{8}$$

For mixed-mode loading, crack initiates when the scalar function of interlaminar stress reaches to the limit where $f_{initiation}$ represents the formulation of interaction of traction.

$$f_{initiation} = f(T_i) - 1 = 0 \tag{9}$$

Under pure mode of loading, crack propagates when the stress reaches to a maximum value in the loading direction. Under mixed mode of loading, the tensile and shear

stress combination determines the damage propagation as shown in Figure 3.2. Various types of damage initiation criteria for mixed mode of loading can be specified.

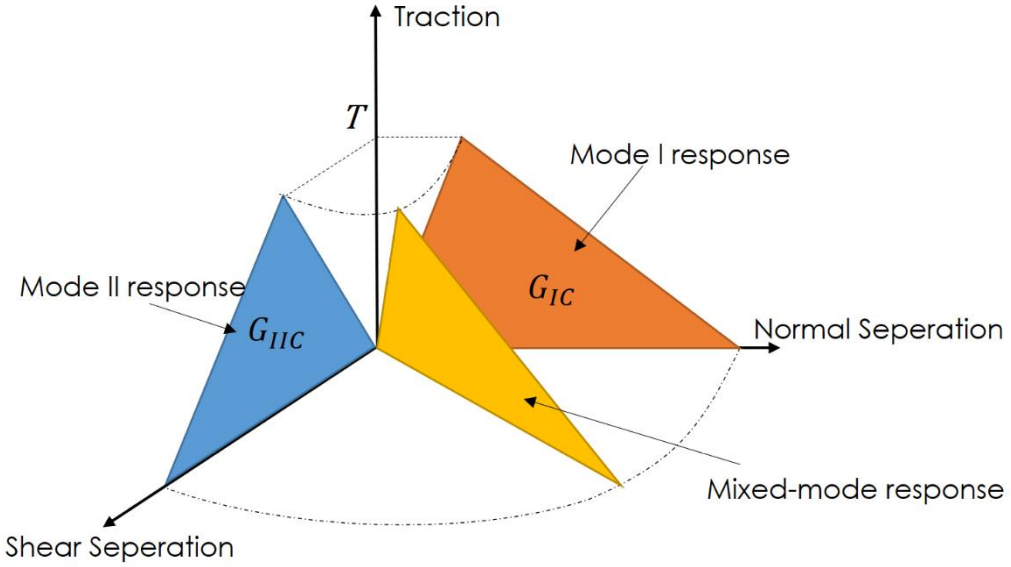

Figure 3.2. Mixed Traction-Separation Law

Cohesive elements are treated with two stress-based-damage-initiation criteria which are Maximum Nominal Stress Criterion (MAXS) and Quadratic Nominal Stress Criterion (QUADS). For both damage criteria, nominal stress to critical stress ratios are used to determine the material response. T_n^0, T_s^0, T_t^0 represents the critical nominal stresses where T_n, T_s, T_t represent current the nominal stress values in pure normal mode, first shear and second shear directions, respectively.

The maximum nominal stress criterion (MAXS) is represented by

$$f_{initiation} = max\left\{\frac{\langle T_n \rangle}{T_n^0}, \frac{T_s}{T_s^0}, \frac{T_t}{T_t^0}\right\} - 1 = 0 \qquad (10)$$

Whereas the quadratic nominal stress criterion (QUADS) is given as

$$f_{initiation} = \left(\frac{\langle T_n \rangle}{T_n^0}\right)^2 + \left(\frac{T_s}{T_s^0}\right)^2 + \left(\frac{T_t}{T_t^0}\right)^2 - 1 = 0 \quad (11)$$

Where "⟨ ⟩" is MacAuley bracket and given by;

$$\langle x \rangle = \frac{1}{2}(x + |x|) \quad (12)$$

In both criteria, the damage initiation is satisfied when the defined criteria reaches to 1 or a higher value. For MAXS criterion, when one of the stress ratios satisfies the criteria, the damage initiates regardless of other stress ratios. For QUADS however, the summation of all three ratios is expected to meet the damage criterion. In summary, there is no relation between different stress directions in MAXS criterion while QUADS criterion combines all three stress directions. If the aim is not the evaluation of the damage criterion then the QUADS damage criterion is beneficial by including all three stresses in the criteria [35].

Damage propagation

Under pure mode of loading, the damage propagation is completed when energy release rate (G_I, G_{II}, G_{III}) reaches to the fracture toughness (G_C) of the material as;

$$G_T = G_C \quad (13)$$

where;

$$G_T = G_I + G_{II} + G_{III} \quad (14)$$

In the mixed mode loading, coupling effects should be taken into account and crack propagation can be expressed with Kenane and Benzeggagh [39] failure criterion;

$$f_{propagation} = \frac{G_T}{G_c} - 1 = 0 \quad (15)$$

G_T can be calculated by using Eq.13 , where calculation of G_c given in below;

$$G_c = G_I^c + (G_{II}^c - G_I^c)\left(\frac{G_{II} + G_{III}}{G_T}\right)^{\eta} \quad (16)$$

where η represents B-K (Benzeggagh- Kenane) parameter for mixed mode loading. It is obtained experimental.

3.1. Traction-Separation Law

Depending on the joint design and materials, the type of traction-separation law causes different results. The selection of the most efficient law type based on adhesive material and joint geometry can help obtaining more accurate results and decreasing computational effort.

3.1.1. Bilinear Traction Law

The bilinear traction separation law is proposed by Alfano and Crisfield in 2006 and it represents the linear softening behavior of a cohesive material [42]. The bilinear law have a triangular shape (Figure 3.3) and it is generally preferred due to its simplicity and good accuracy for specially brittle materials.

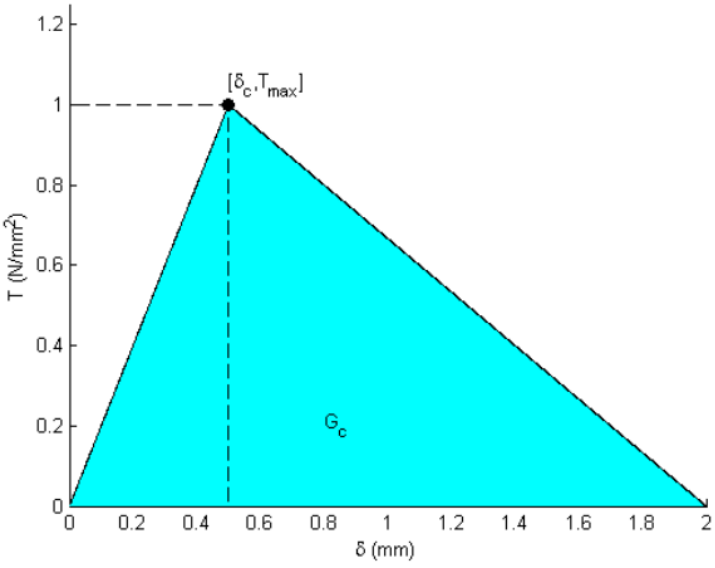

Figure 3.3. Bilinear Traction-Separation Law[5]

Ductile materials are well represented by using trapezoidal law[40]. Tvergaard and Hutchinson [41] first introduced this traction behavior and it closely approximates experimental results. Although it is a preferable method for such materials, convergence problems are higher in trapezoidal law considering the other traction behaviors.

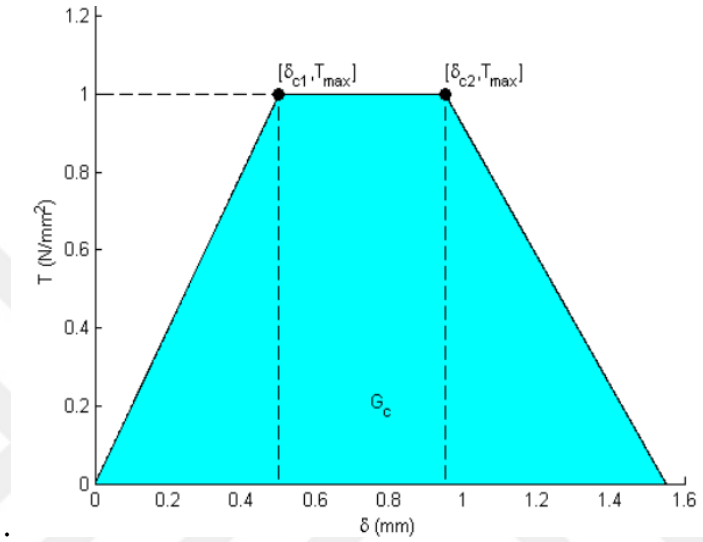

Figure 3.4. Trapezoidal Traction-Separation Law [5]

3.1.2. Exponential Traction Law

Exponential law is the most advantageous one in CZM due to its high accuracy and low computational cost. The exponential law function has continuous tractions which provides easy implementation and ease of computation[5]. This is proposed by Xu and Needleman and an example of exponential law is given in Figure 3.5 [32].

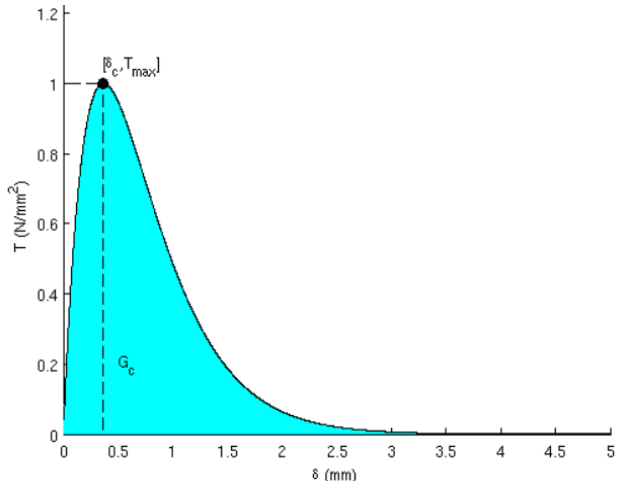

Figure 3.5. Exponential Traction-Separation Law[3]

CHAPTER 4

METHODOLOGY

4.1. Single Lap Joint Test

In the scope of this thesis study, a single lap joint test campaign has been conducted. The behavior of adhesive bonded joints with various adherend thicknesses and adhesive joint lengths are aimed to be investigated. ASTM 3165 standard test is performed to investigate single-lap-joint test specimens with 12 different joint configurations.

4.1.1. Material Specifications

Paste adhesive Hysol EA9394 is used as a bonding agent between the top and bottom adherends. Adhesive thickness is kept constant with 1mm for all configurations. Adherends are created by using fabric plies or both fabric and UD plies. For fabric, HexPly 8552S/37%/280H5 material is selected, while AS4/8552 RD34 AW194 is selected for UD material. Adhesive, UD and fabric material properties are defined in Table 4.1, Table 4.2 and Table 4.3.

Table 4.1. *EA9394 paste adhesive property table*

Property	E_1 **[GPa]**	E_2 **[GPa]**	E_3 **[GPa]**	t_n **[MPa]**	t_s **[MPa]**	t_t **[MPa]**	G_{Ic}	G_{IIC}	G_{IIIc}
Value	2.7	1.0	1.0	46	28.9	28.9	100	160	160

Table 4.2. *Hexply (8552S/37%/280H5) property table*

Property	E_1 **[GPa]**	E_2 **[GPa]**	υ_{12}	G_{12} **[GPa]**	G_{13} **[GPa]**	G_{23} **[GPa]**
Value	62	62	0,05	4.2	4.2	4.2

Table 4.3. *UD (AS4/8552 RD34 AW194) property table*

Property	E_1 [GPa]	E_2 [GPa]	υ_{12}	G_{12} [GPa]	G_{13} [GPa]	G_{23} [GPa]
Value	135	8.5	0.35	4.2	4.2	4.2

4.1.2. Test Configurations

Test specimen representation and configurations are shown in Figure 4.1. Notches created on top and bottom have 3mm length. Adhesive thickness and adherend width are 1mm and 25mm, respectively for all specimens. Adherend thickness, adherend length and bond length vary according to the test specimen configuration.

Top and bottom adherends are not identical in any test configuration. Both have different thicknesses and different stacking sequences. 12 different configurations which are defined by Turkish Aerospace Industries to represent a structural joint in practice are used in the test program. A notation given in Figure 4.2 is defined for each configuration. Thickness and sequence of the adherends are given in Table 4.4.

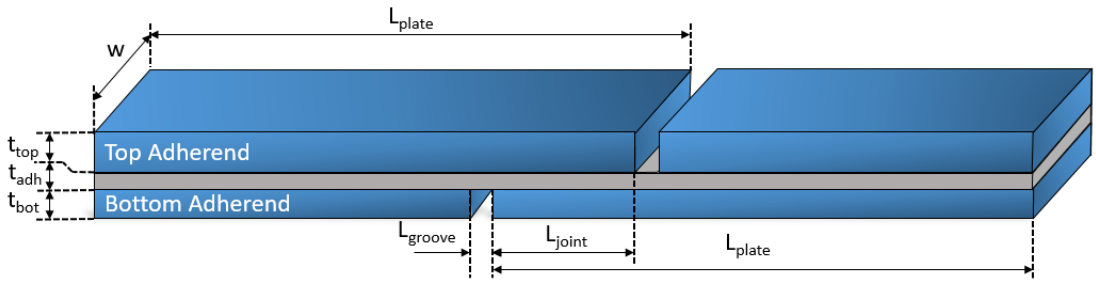

Figure 4.1. Representation of SLJ test configuration

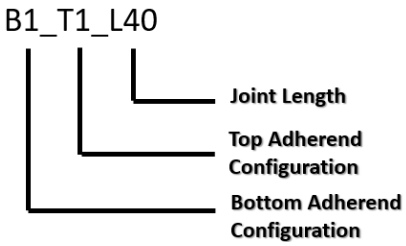

Figure 4.2. Test Specimen Notation

Table 4.4. *Test Specimen Stacking Sequence and Thickness*

No	*Bottom adherend*	*Top adherend*	L_{joint} *[mm]*	L_{plate} *[mm]*	*Bottom Adherend Thickness [mm]/Sequence*	*Top Adherend Thickness [mm]/Sequence*
1	**B1**	**T1**	**24**	**107**	**4.12**	**12.79**
					[45/0/45/0/45/$(0)_2$/45/0/45/0/45**/0/45**]*	[$(45)_2$/0/0/45/0/135/0/45/0/45/0/0/0/135/$(0)_2$/0/0/45/0/45/0/$(0)_2$/$(0)_2$/0/0]$_s$
2	**B2**	**T2**	**28**	**111**	**2.44**	**8.86**
					[45/0/$(45)_2$/0/45**/0/45**]*	[$(45)_2$/$(0)_2$/135/$(0)_2$/45/$(0)_2$/135/$(0)_2$/0/$(0)_2$/45/$(0)_3$/0/(0)]$_s$
3	**B2**	**T3**	**28**	**111**	**2.44**	**7.76**
					[45/0/$(45)_2$/0/45**/0/45**]*	[$(45)_2$/$(0)_2$/135/$(0)_2$/45/0/135/0/0/($0)_2$/45/$(0)_2$/0/0]$_s$
4	**B3**	**T4**	**40**	**123**	**2.44**	**7.76**
					[45/0/$(45)_2$/0/45**/0/45**]*	[$(45)_2$/$(0)_2$/135/$(0)_2$/45/0/135/0/0/($0)_2$/45/$(0)_2$/0/0]$_s$
5	**B3**	**T11**	**28**	**111**	**2.44**	**5.55**
					[45/0/$(45)_2$/0/45**/0/45**]*	[$(45)_2$/0/135/0/45/$(0)_2$/0/$(0)_2$/0/0]$_s$
6	**B4**	**T12**	**26**	**109**	**1.6**	**5.55**
					[45/0/45**/0/45**]*	[$(45)_2$/0/135/0/45/$(0)_2$/0/$(0)_2$/0/0]$_s$
7	**B5**	**T6**	**40**	**123**	**1.6**	**5.55**
					[45/0/45**/0/45**]*	[$(45)_2$/0/135/0/45/$(0)_2$/0/$(0)_2$/0/0]$_s$
8	**B5**	**T7**	**40**	**123**	**1.6**	**4.62**
					[45/0/45**/0/45**]*	[$(45)_2$/0/135/0/45/$(0)_3$/0/0]$_s$
9	**B5**	**T8**	**40**	**123**	**1.6**	**3.15**
					[45/0/45**/0/45**]*	[$(45)_2$/$(0)_3$/0/0]$_s$
10	**B5**	**T9**	**40**	**123**	**1.6**	**2.50**
					[45/0/45**/0/45**]*	[$(45)_2$/$(0)_3$/0/$(0)_3$/$(45)_2$]
11	**B5**	**T10**	**40**	**123**	**1.6**	**1.49**
					[45/0/45**/0/45**]*	[$(45)_2$/0]$_s$
12	**B6**	**T5**	**24**	**123**	**4.68**	**12.78**
					[45/0/45/0/45/0/45/45/0/45/0/45**/0/45**]*	[$(45)_2$/0/0/45/0/135/0/45/0/45/0/0/0/135/$(0)_2$/0/0/45/0/45/0/$(0)_2$/$(0)_2$/0/0]$_s$

Note : Underlined plies refer to UD. Rest are fabric plies.
*** Highlighted [0/45] plies are applied in second cure.**

4.1.3. Preparation of Test Specimens

Specimens are composed of UD (8552/34%/UD194/AS4) and fabric (Hexply 8552e/37%280H5). Top adherends with different laminate sequences are all manufactured by co-curing process using both UD and fabric plies during the lamination. While only fabric plies are used in bottom adherends manufactured by co-bonding. A number of fabric plies are stacked and cured in autoclave followed by adding wet fabric plies on cured plies by using an adhesive material. The laminates are cured in autoclave once again as the final treatment. The structure of top and bottom adherends are shown in Figure 4.3.

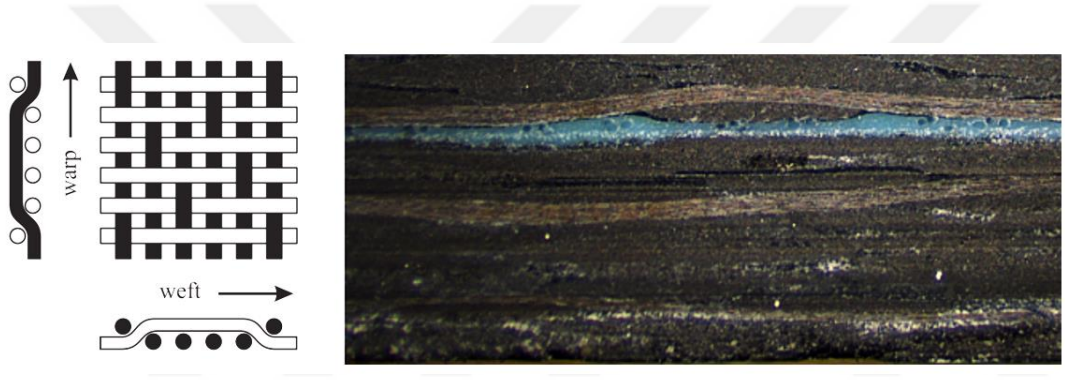

a) Bottom adherend configuration with 5HS co-bonded laminate

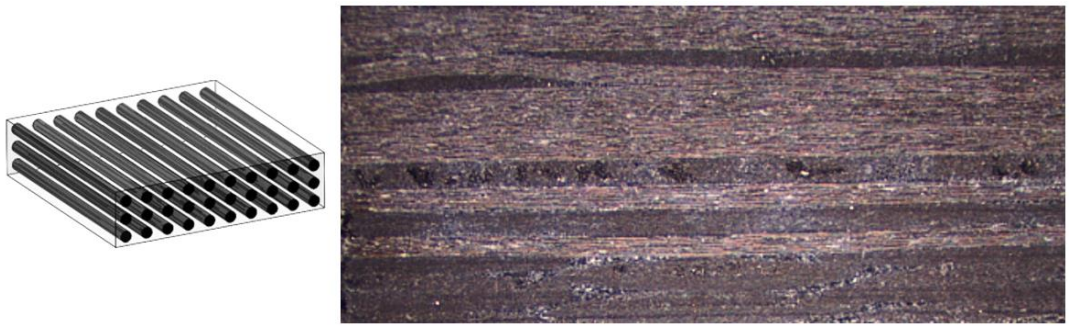

b) Top adherend configuration with UD and 5HS co-cured laminate

Figure 4.3. Top and bottom adherends stacking configuration

Later, adherend sheets are bonded together by using bonding agent which is EA9394 paste adhesive in secondary bonding procedure. The selected type of adhesive allows curing at room temperature in 3 to 5 days as well as the procedure may be accelerated by heating up to 93°C [LOCTITE EA 9394 AERO 9-2013]. In the specimen preparation, the room-temperature curing procedure is followed to bond pre-cured laminates.

Specimens are trimmed in accordance with Figure 4.4 and test specimens are cut in final shape as shown in Figure 4.1. A total of 8 specimens obtained from each bonded sheet. Notches are created carefully in the purpose of not to scratch the sheets under the notch and have notches of right angle with respect to the longitudinal direction of the specimen.

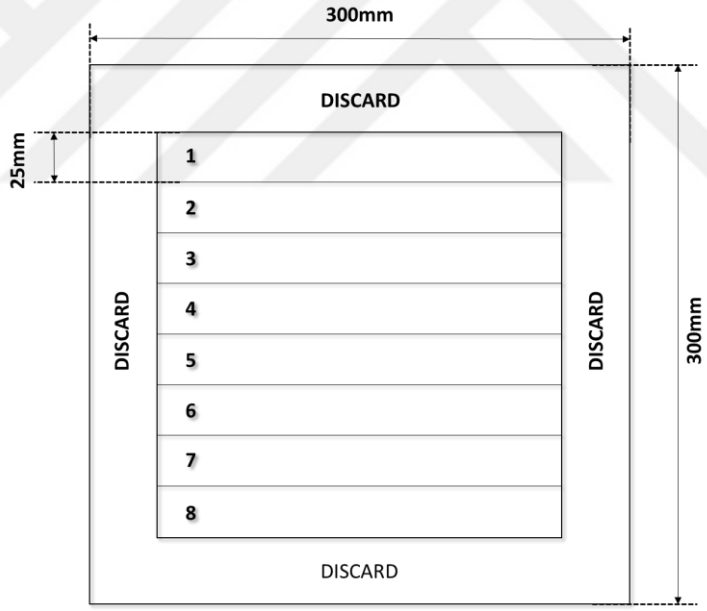

Figure 4.4. Trimmed sheet plate

4.1.4. Test Method

ASTM D-3165 “Strength Properties of Adhesives in Shear by Tension Loading of Single-Lap-Joint Laminated Assemblies” [29] is used as the standard test method which is followed to obtain shear strength values of adhesive.

In the test procedure, two plates are bonded with an adhesive followed by grooving performed on laminated assembly.

Testing is performed by loading the end of the single lap joint with tension as represented in Figure 4.5.

Two self-aligning grips are set to hold the specimen. Grips are aligned from starting point of the notches to minimize the bending effect generated due to eccentricity in loading. The test machine configuration is schematically shown in Figure 4.6. The rate of loading of the test machine is set to 1 mm/min. Test is proceeded until a 40% reduction in load after failure.

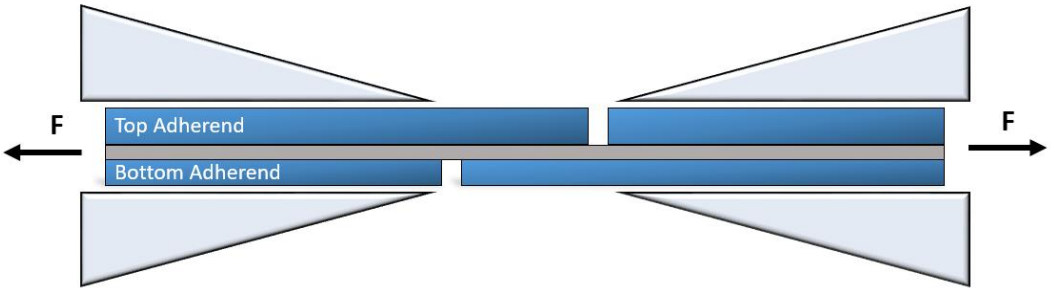

Figure 4.5. Single lap joint test loading condition

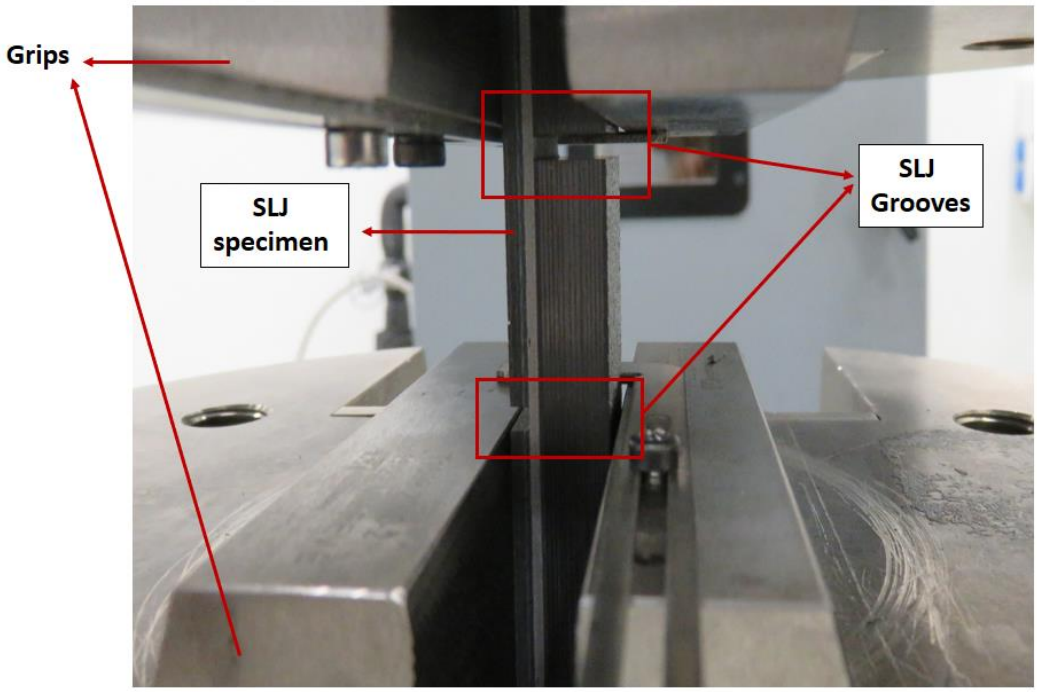

Figure 4.6. Single lap joint test machine

4.2. Finite Element Modelling

Finite element model of the single lap joint is implemented in ABAQUS/CAE (SIMULA™ by Dassault Systèmes®) where a non-linear implicit analyses performed by using Abaqus/Standard.

A three-dimensional model is employed to capture the out of plane stress distribution and bending effects formed in the single lap joint. Instead of modelling full length of the adherends, only the partial volume beyond clamping is modelled as shown in Figure 4.7. By this way, a considerable reduction in computational time is aimed. Modelling performed by using the *x* axis representing as the longitudinal, *y* axis as the width, and *z* axis as the thickness directions of the specimen.

Top and bottom adherends, adhesive and adhesive interfaces are each modelled separately. Cohesive elements at the interface and continuum shell elements for bulk

adhesive and adherends are used. According to Abaqus Documentation [36] it is emphasized that using conventional shell elements in conjunction with cohesive elements may affect the bending behavior of the model due to contact formulation of continuum shell elements. For this reason, instead of conventional shell elements, continuum shell elements are suggested to be used in models that have interface with cohesive elements.

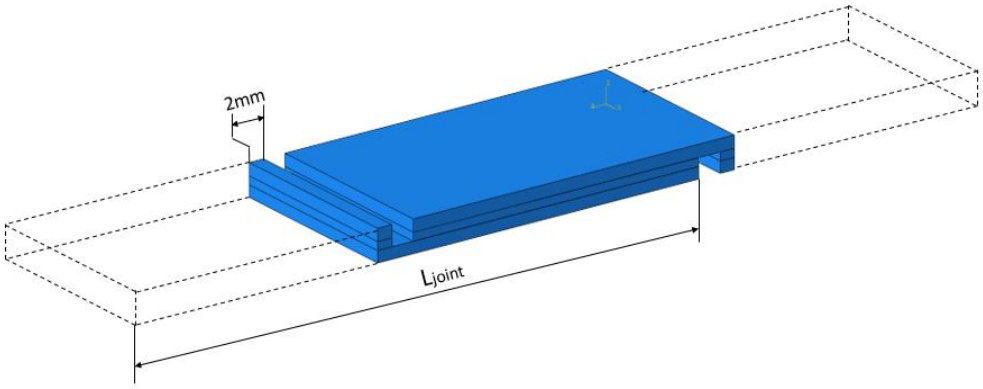

Figure 4.7. Partial modelling of SLJ

In modelling of adherends, 8-node continuum shell elements with reduced integration, S8CR is used. 0.5mm element size defined for all top and bottom adherend configurations. Clamped adherend surfaces are not modeled with full size to save computation time, and boundary conditions are used for simulating clamps. Adhesive bond of single lap joint is simulated as a bulk material which is meshed with continuum shell element, S8CR, same as the adherends.

To simulate the interface crack, cohesive elements are placed between interface of the adhesive bulk material and adherends as shown in Figure 4.8. COH3D8 cohesive element with 8 nodes and 4 integration points are used for interface elements. Exponential behavior for traction-separation law is selected for the adhesive. Interface stiffness is chosen larger than the nominal stiffness as it is suggested in literature [18] to overcome the convergence issues. Quadratic nominal stress criterion (QUADS) is selected as the damage initiation criteria since it assumes a stress relation considering different directions. The critical energy release rate is found by Benzeggagh-Kenane (BK) mixed-mode crack growth criterion.

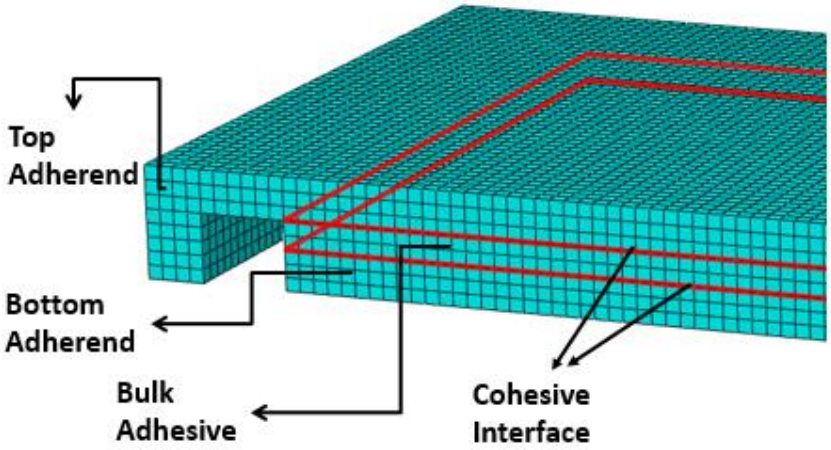

Figure 4.8. SLJ element model

For an optimum mesh size of the cohesive elements, a mesh refinement study is performed on single lap joints in which 6 different mesh sizes are used for the modelling of the interface. The maximum load that joint experiences is compared with respect to the mesh refinement in Figure 4.9 where an asymptotic behavior emerges. However, during the analyses, computational time increases excessively for 0.1-mm mesh size. For that reason, cohesive elements are meshed with 0.25-mm elements. This element size is taken as the optimum value with the consideration of the computational time and the convergence to maximum load.

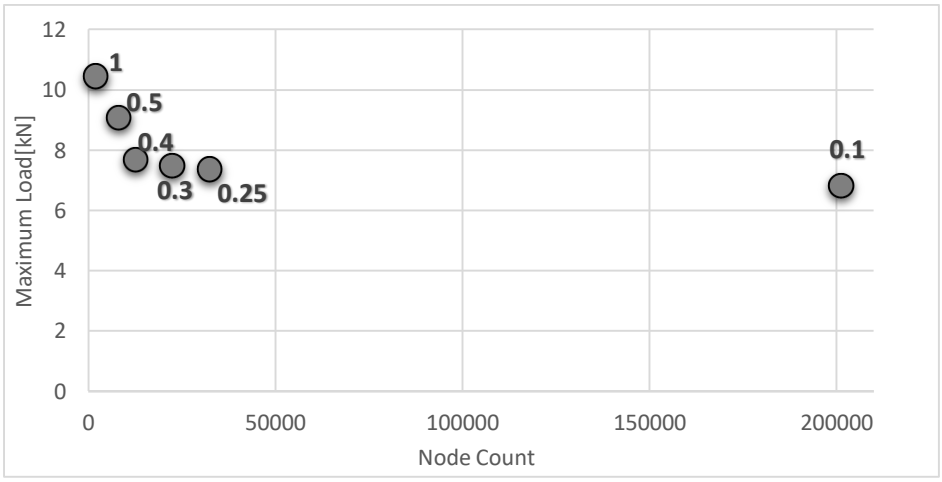

Figure 4.9. Mesh Refinement (Element sizes are in [mm])

As shown in Figure 4.10, interface regions are meshed with elements of finite thickness. Later top and bottom nodes are translated to provide zero thickness elements through the thickness direction.

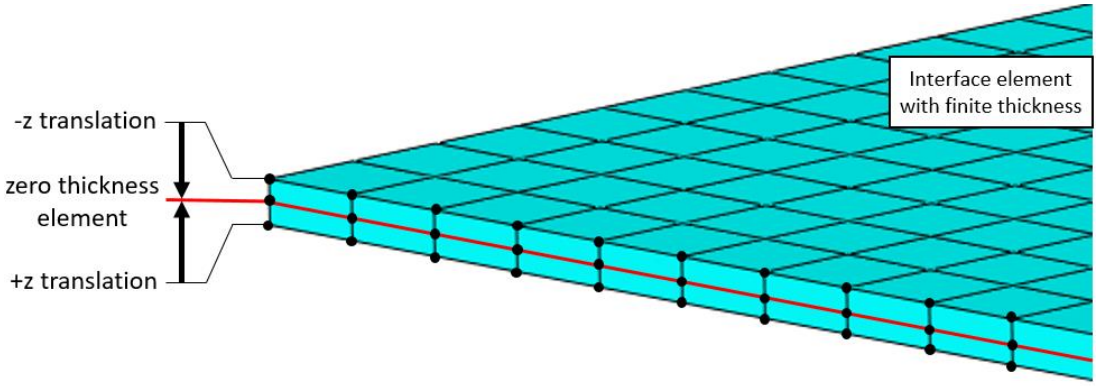

Figure 4.10. Cohesive interface model

4.2.1. Boundary Conditions

Surfaces at the end of each adherend is modelled as fixed. From the end of the other adherend, displacement is defined in *x*-direction. Translations and rotations in *y*- and *z*-directions are prevented along the top and bottom surfaces of the adherend.

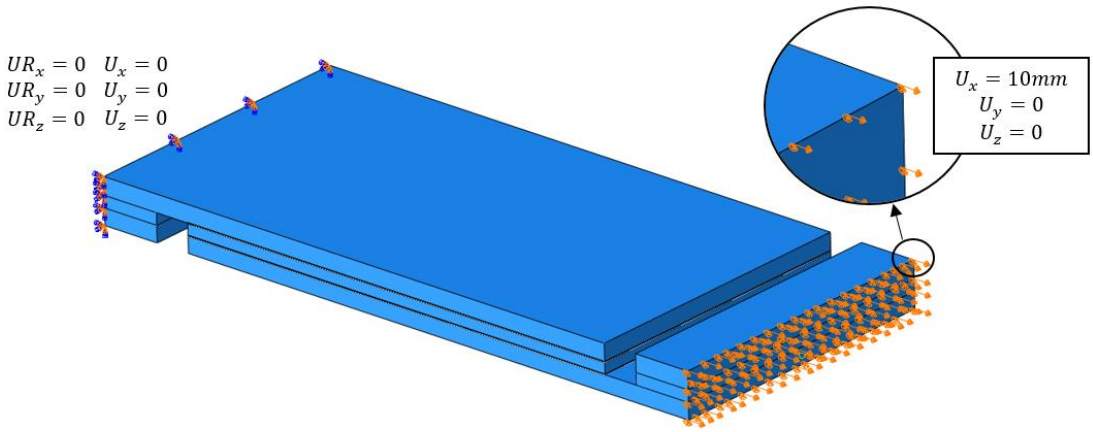

Figure 4.11. Single lap joint boundary condition

CHAPTER 5

RESULTS AND DISCUSSIONS

This study is aimed to investigate mechanical behavior of adhesively bonded single lap joints by conducting a mechanical test program and finite element study. In this chapter, results obtained in experimental study and FEM are elaborated in detail.

The discussion of the results obtained in this study can be classified as follows:

- Microscopic examination to investigate failure modes observed in test specimens
- Observation of damage initiation and propagation with high speed camera
- Effect of single lap joint parameters
- Finite element modeling for the analysis of failure behavior in bonded joints

5.1. Experimental Results

Single lap joint tests are performed for 12 different configurations of composite adherends. The joints are loaded until a 40% load drop is observed due to failure. Maximum load values that the specimens withstand are read from test machine. In order to obtain reliable results, at least 6 specimens for each configuration are used. The mean load values and the standard deviations are calculated for each configuration from measured loads.

Test configurations are classified in such a way that the comparisons of the results are made easy. These classifications are according to identical bottom adherends and joint lengths. Maximum load and shear strength values are given in Table 5.1 - Table 5.3. Load and displacement comparison for classified specimens are given in Figure 5.1 to Figure 5.3.

Table 5.1. *Load and shear strength of specimens with bottom adherend thickness =1.6mm Ljoint=40mm*

Name	Max Load [kN]			Shear Strength [MPa]			Bottom thickness[mm] /sequence		Top thickness [mm]/sequence
	max	min	mean	max	min	mean			
B5_T10_L40	12.09	6.63	7.97	11.93	6.57	7.87	1.6	[45/0/45/0/45]	1.49
									$[(45)_2/\underline{0}]_s$
Standard Dev	0.48			0.47					
B5_T9_L40	11.77	7.96	8.87	11.69	7.90	8.81			2.50
									$[(45)_2/(\underline{0})_3/0/(\underline{0})_3/(45)_2]$
Standard Dev	0.40			0.39					
B5_T8_L40	11.63	9.94	10.65	11.74	9.95	10.67			3.15
									$[(45)_2/(\underline{0})_3/0/\underline{0}]_s$
Standard Dev	0.70			0.72					
B5_T7_L40	16.39	11.95	13.13	16.17	11.90	13.02			4.62
									$[(45)_2/\underline{0}/\underline{135}/\underline{0}/\underline{45}/(\underline{0})_3/0/\underline{0}]_s$
Standard Dev	0.44			0.43					
B5_T6_L40	10.99	9.95	10.55	10.94	9.85	10.45			5.55
									$[(45)_2/\underline{0}/\underline{135}/\underline{0}/\underline{45}/(\underline{0})_2/0/(\underline{0})_2/0/\underline{0}]_s$
Standard Dev	0.17			0.19					

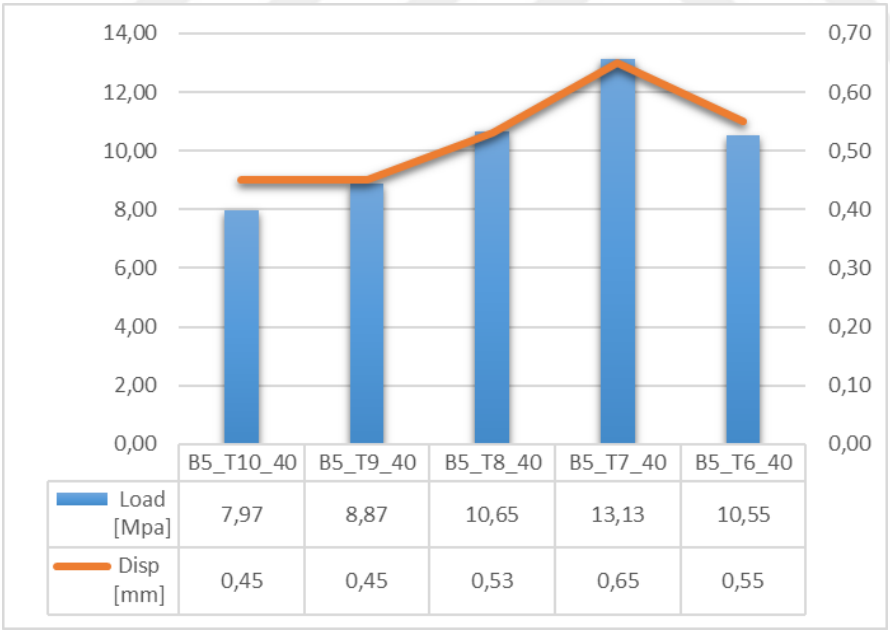

Figure 5.1. Load-displacement comparison for bottom adherend thickness =1.6mm L=40mm

Table 5.2. *Load and shear strength of specimens with bottom adherend thickness =2.44mm Ljoint =28mm*

Name	Max Load [kN]			Shear Strength [MPa]			Bottom thickness[mm] /sequence		Top thickness [mm]/sequence
	max	min	mean	max	min	mean			
B3_T11_L28	14.37	10.65	11.69	20.38	15.03	16.60	2.44	[45/0/(45)2/0/45/0/45]	5.552 [(45)₂/0/135/0/45/(0)₂/0/(0)₂/0/0]ₛ
Standart Dev	0.44			0.69					
B2_T3_L28	15.79	14.48	14.94	22.10	20.36	21.06			7.76 [(45)₂/(0)₂/135/(0)₂/45/0/135/0/0/(0)₂/45/(0)₂/0/0]ₛ
Standart Dev	0.47			0.64					
B2_T2_L28	18.47	15.47	16.63	26.09	21.44	23.31			8.864 [(45)₂/(0)₂/135/(0)₂/45/(0)₂/135/(0)₂/0/(0)₂/45/(0)₃/0/(0)]ₛ
Standart Dev	0.32			0.56					

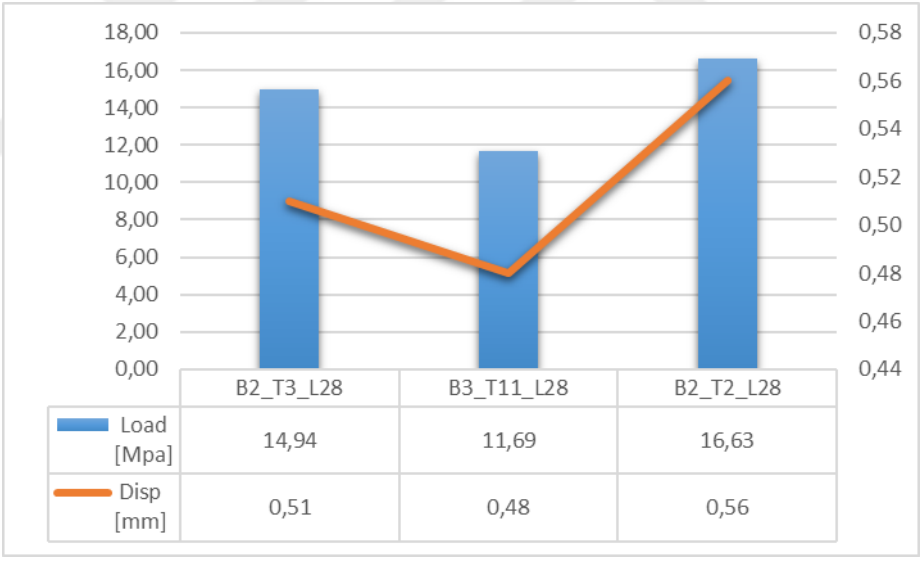

Figure 5.2. Load-displacement comparison for bottom adherend thickness =2.44mm L=28mm

Table 5.3. *Load* and shear *strength of specimens with bottom adherend thickness =4.12mm Ljoint=24mm*

Name	Max Load [kN]			Shear Strength [MPa]			Bottom thickness[mm] /sequence	Top thickness [mm]/sequence	
	max	min	mean	max	min	mean			
B1_T1_L24	12.24	10.88	11.66	20.33	18.11	19.38	4,12 [45/0/45/0/45/(0)2/45/0/45/0/45/0/45]	12,784	[(45)2/0/0/45/0/135/0/45/0/45/0/0/0/135/(0)2/0/0/45/0/45/0/(0)2/(0)2/0/0]s
Standart Dev	0.48			0.78					
B6_T5_L24	15.70	13.07	14.64	27.18	22.67	25.37	4,68 [45/0/45/0/45/0/45/45/0/45/0/45/0/45/0/45]		
Standart Dev	0.54			0.93					

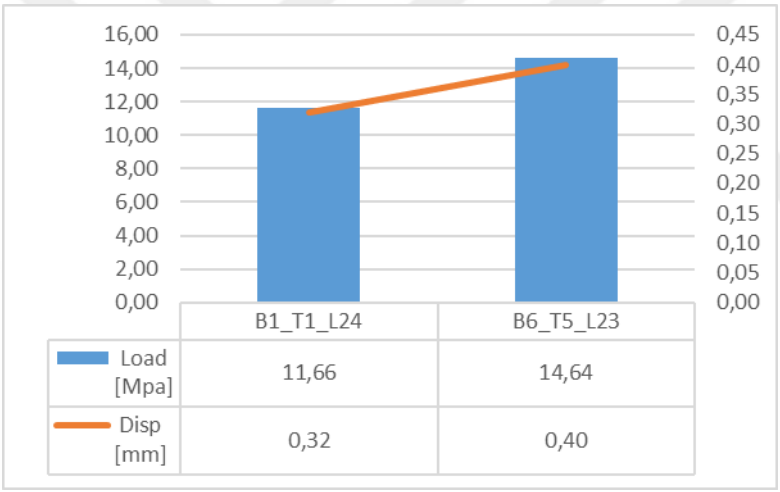

Figure 5.3. Load-displacement comparison for bottom adherend thickness =4.12mm L=24mm

5.1.1. Failure Modes

Microscopic examinations are performed to detect the failure modes that take place in single lap joints. For the examination, 4 different test configurations are selected which can be used for generalizing on failure modes for the remaining configurations. The selected configurations and adherend sequences are given in Table 5.4. Three specimens for each configuration are examined under the microscope to make accurate

decisions on failure modes. Also, for those selected configurations on which the microscopic analyses are carried out, the load-displacement curves of one of the specimens from each configuration are presented in Figure 5.4.

Table 5.4. *Selected specimen configurations for microscopic examination*

	Bottom adherend thickness [mm]/ Sequence	***Top adherend thickness [mm]/ Sequence***
B2_T2_L28	2,44	8,864
	[45/0/(45)$_2$/0/45/0/45]	[(45)$_2$/(0)$_2$/135/(0)$_2$/45/(0)$_2$/135/(0)$_2$/0/(0)$_2$/45/(0)$_3$/0/(0)]$_s$
B3_T11_L28	2,44	5,552
	[45/0/(45)$_2$/0/45/0/45]	[(45)$_2$/0/135/0/45/(0)$_2$/0/(0)$_2$/0/0]$_s$
B5_T6_L40	1,6	5,552
	[45/0/45/0/45]	[(45)$_2$/0/135/0/45/(0)$_2$/0/(0)$_2$/0/0]$_s$
B5_T10_L40	1,6	1,488
	[45/0/45/0/45]	[(45)$_2$/0]$_s$

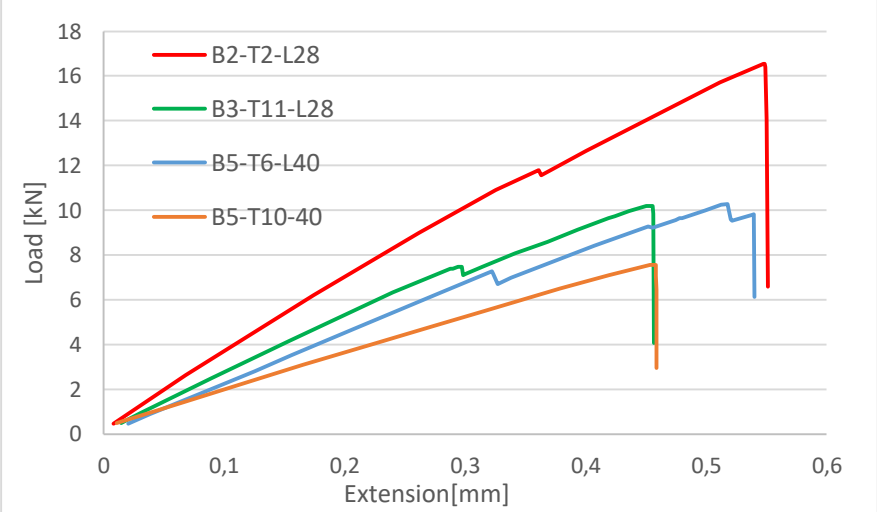

Figure 5.4. Load-displacement curve

Regardless of joint length or adherend stiffness, the same failure mode is observed in all four configurations. Crack initiates at the end of the overlap of SLJ specimen where tensile stresses are dominant and it propagates towards to the overlap where the area under compression as shown in Figure 5.5. This crack behavior can be explained in Karachalios paper [10]. Since the adhesive material is stronger in compression than in

tension, crack initiates where the tension load is dominant. Then the crack propagates along the overlap interface until it jumps through the adhesive to the upper interface. Angular crack formation in all specimens is evaluated as an expected product of the bending effect.

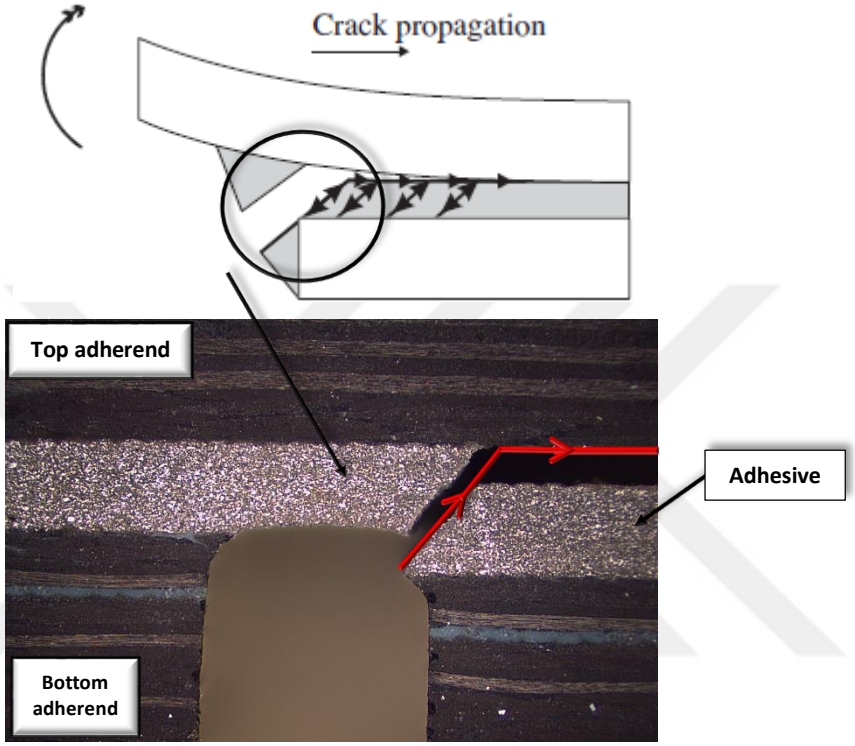

Figure 5.5. Failure mechanism in SLJ

The examination of adhesive bonded composite joints are represented in Figure 5.9 - Figure 5.12. The resolution, magnification and other inspection set-ups of the microscope are given in Figure 5.7. Examinations are performed for both ends and middle section of SLJ, where photographs are taken at three sections as shown in Figure 5.8. Here, only one specimen from each configuration is presented. Remaining representations are given in Appendix B. In spite of the same failure mode (adhesive failure mode) taking place, there are some discrepancies in failure behavior among specimens within the same configuration. For example, damage in fabric plies can be observed as shown in Figure 5.6. This difference in failure behavior can be due to unwanted flaws which are formed during the manufacturing process.

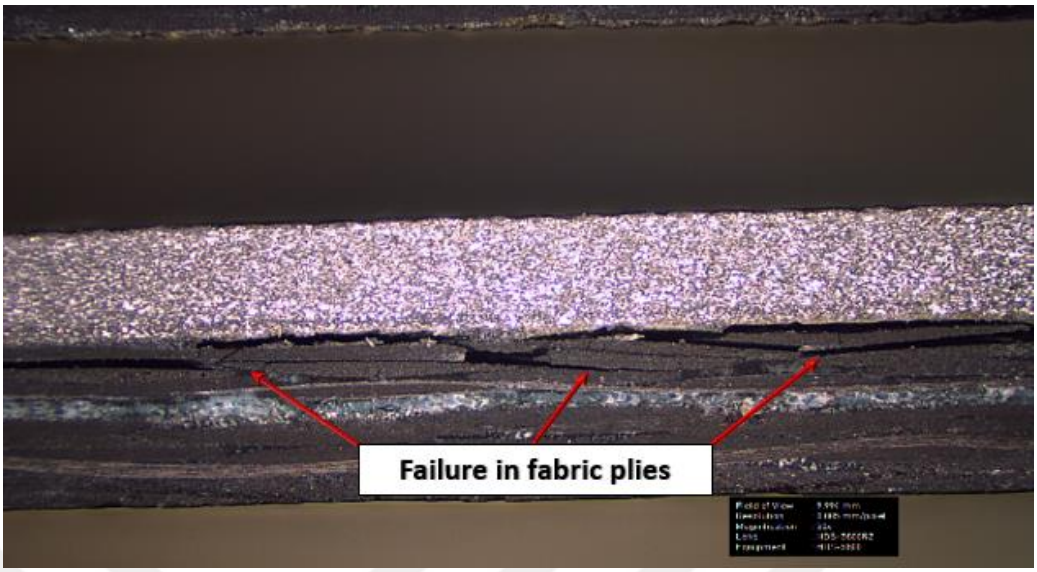

Figure 5.6. Test specimen representation

With a detail examination of Figure 5.10 and Figure 5.12, one can arrive at various conclusions for crack initiations. As shown in Figure 5.10 for Specimen B3_T11_L28 the crack initiates from only one side. It propagates through the adhesive in an angular form until the opposite adherend surface. Then, it continues to propagate along the interface of the overlap.

A distinctive failure mechanism exists in Specimen *B5_T10_L40*. As seen in Figure 5.12 crack initiates at both ends of the overlap. No crack jump is observed since no proper breakup is seen in the adhesive. Different from the two mentioned configurations for the specimens shown in Figure 5.9 and Figure 5.11 there is not enough evidence to conclude about the crack initiation and propagation behavior since multiple angular failure in adhesive is observed.

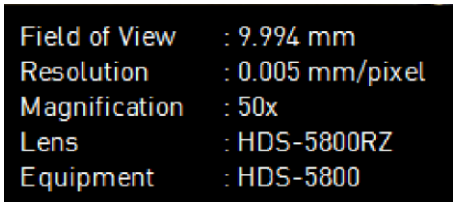

Figure 5.7. Scale of the microscopic examination

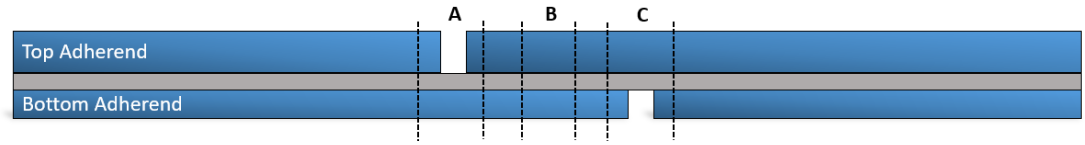

Figure 5.8. Test specimen representation

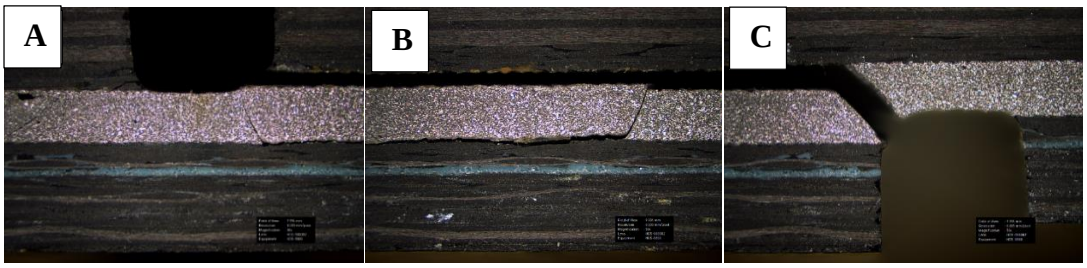

Figure 5.9. Three sections of B2_T2_L28 (Test specimen 1)

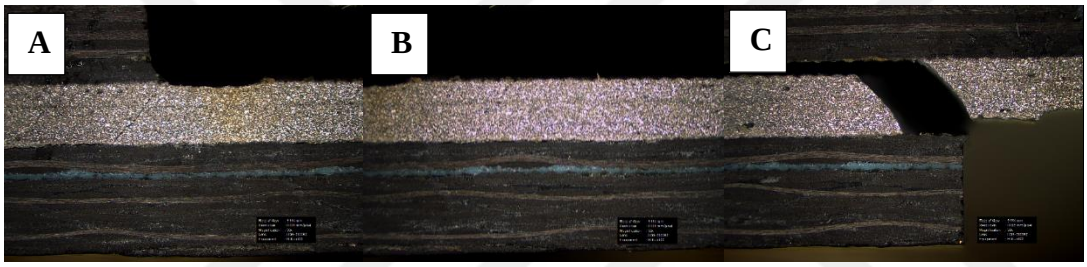

Figure 5.10. Three sections of B3_T11_L28 (Test specimen 3)

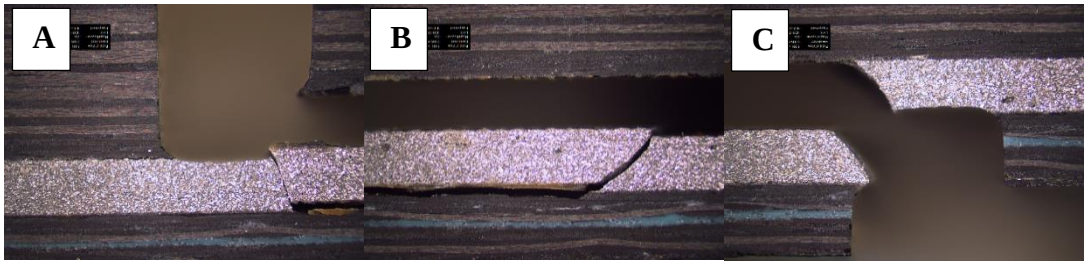

Figure 5.11. Three sections of B5_T6_L40 (Test specimen 1)

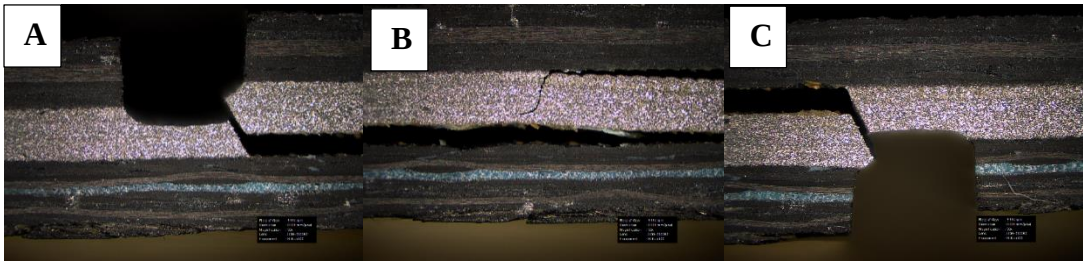

Figure 5.12. Three sections of B5_T10_L40 (Test specimen 3)

5.1.2. High-Speed Video Test

Thereafter microscopic examination, it is concluded that already cracked specimens do not give an idea about crack initiation and propagation while it is helpful to designate of the failure modes only. In order to determine the crack initiation and propagation behavior of SLJ specimens, a mechanical SLJ test repeated by recording with a high-speed camera for Specimen *B5_T8_40*. Test setup for this experiment is given in Figure 5.13.

The SLJ specimen is placed between clamps of the servo-hydraulic test machine. A constant 1 mm/min displacement is applied and a force reduction tolerance of 40% is defined in test machine similar to previous tests. Clamp forces are adjusted to 40 MPa at first. However, slipping of the specimens between clamps are observed during the test due to relatively low roughness of the clamp surfaces. Friction is increased with the use of pasting sandpaper glued to the composite specimen at the location where there is an interface with clamps of the test machine. Also clamp forces increased to 45 MPa to ensure proper holding.

From one side of the specimen, a high speed camera is set to record the experiment. The camera is employed 140,000 frame per second capture rate and two flood lights are used to have necessary illumination for such high speed filming.

Figure 5.13. SLJ test and high-speed camera setup

Even if the very similar specimen which is cut from the same plate is used in the high speed camera test, the load-displacement result is compared with the results of previously testes 6 specimens of *B5_T8_40* configuration to ensure the consistency with similar previous experiments since high-speed camera test is performed on a different test machine. The comparison (Figure 5.14) shows that a relatively higher stiffness is obtained from high-speed camera test. Even so it can be concluded that fairly enough coherence obtained on the crack initiation and propagation behavior.

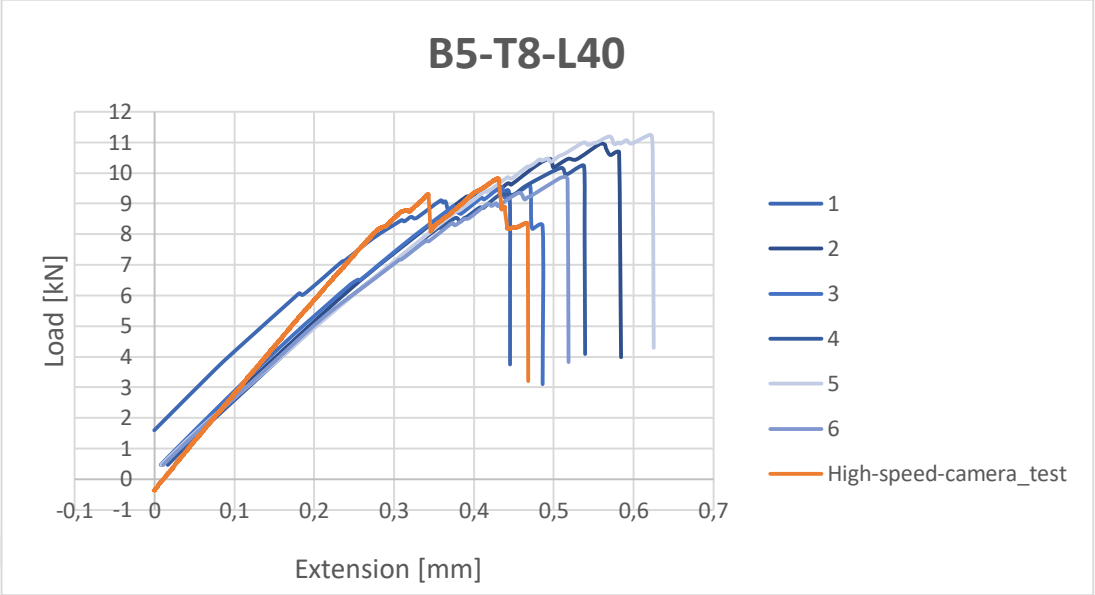

Figure 5.14. Comparison test results

The crack initiation and propagation photographs are given in Figure 5.15 in three steps. During the experiment, only a limited interval of crack behavior can be recorded with high speed camera since the camera has the capability of recording only 2 seconds before and 2 seconds after the crack initiation. Because the full damage after crack initiation lasts more than 2 seconds, the whole damage progression could not be captured by the camera. However, it can be concluded that, crack initiates from the thicker part of the unbalanced configuration in contrast to the conclusions in Kutscha and Hofer paper [12] where the crack initiation observed at the end of thinner adherend because of maximum shear stress developed in that area.

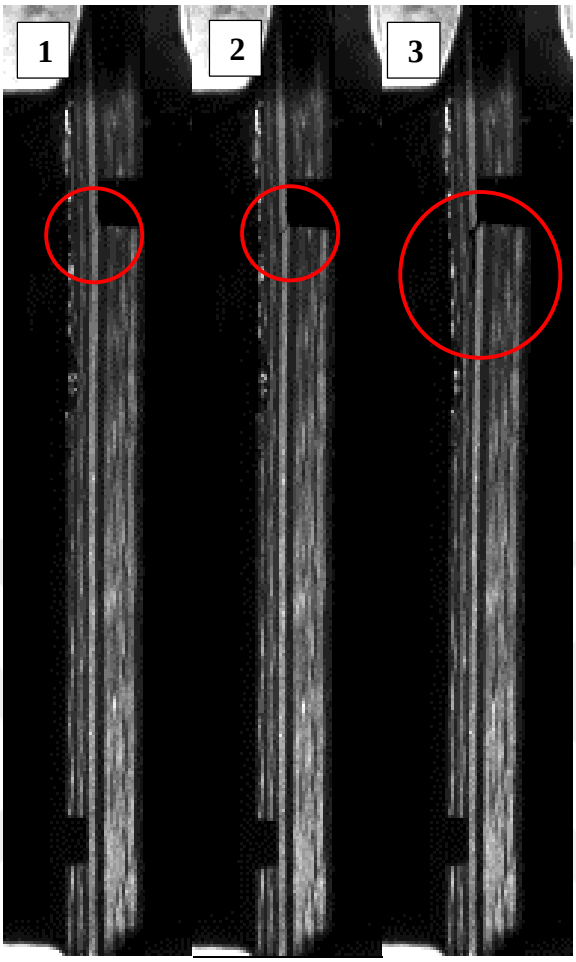

Figure 5.15. Step by step crack propagation

In the Figure 5.16 the un-cracked and cracked specimens are shown. The crack propagated through the interface of the adhesive and adherend until the middle part of the overlap. In the middle, a sharp crack jump is observed along the adhesive thickness direction. After crack jumps, it may propagate through the other side of the interface or a new crack initiates at the opposite end of the overlap and it propagates until it coalesces with a previous crack. However, it cannot be concluded which of the scenarios take place in reality since a limited duration of crack propagation is captured with high speed camera which does not give enough detail.

Figure 5.16. Uncracked and cracked specimen

A detailed crack examination is presented in Figure 5.17. Adhesive which is remained on the top adherend is broken into two pieces at the middle of the overlap. Smooth crack interface cannot be detected since the trace of the 45° fabric plies of the adherends exist adjacent to the adhesive. However, there is no full ply removal that can be observed and only a thin surface of the upper ply of the adherends is observed to be still bonded to the adhesive during the separation.

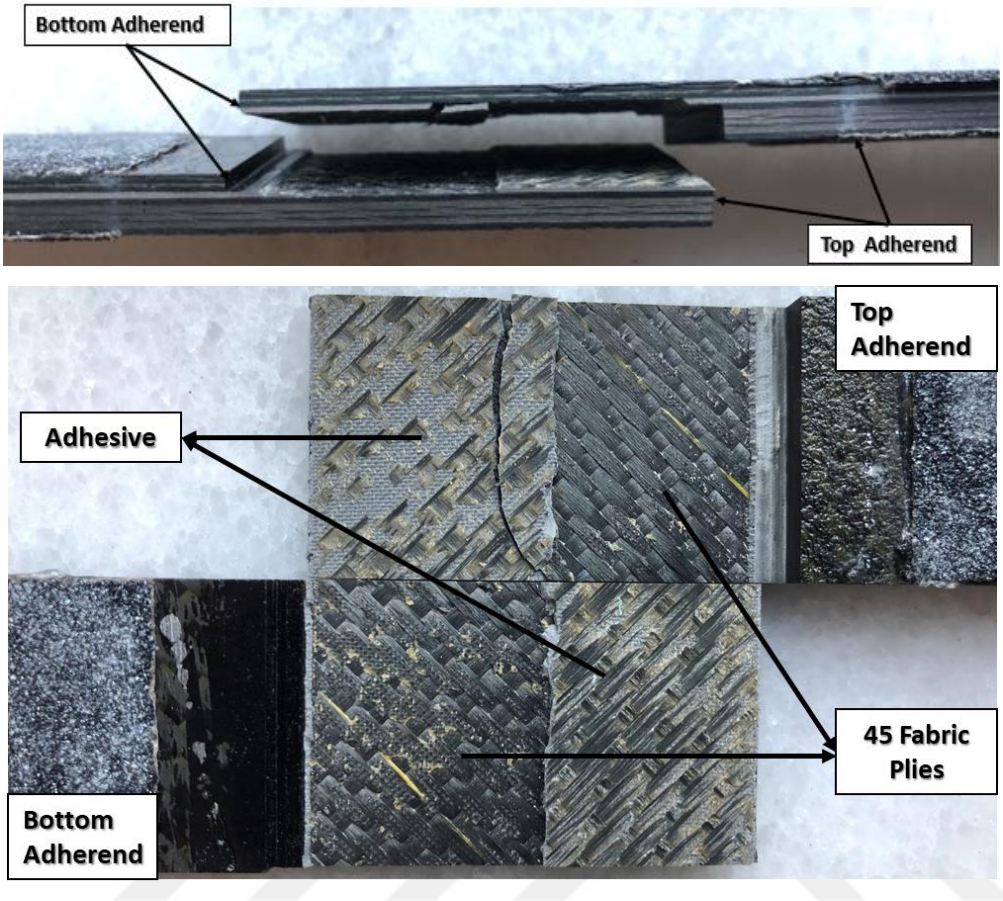

Figure 5.17. Detailed examination of cracked specimen

5.1.3. Effects of Bending Stiffness

Stiffness increase in composite specimens is shown to provide a higher joint efficiency. When bending stiffness of the adherend increase, the bending curvature in specimens decreases in return. Thus, resulting peel stress decreases for stiff laminates and this leads to an increase in joint strength [11]. The classical lamination theory (CLT) is used to calculate the bending stiffness in longitudinal direction. Bending moment is calculated as;

$$\begin{bmatrix} M_x \\ M_y \\ M_{xy} \end{bmatrix} = \begin{bmatrix} B_{11} & B_{12} & B_{16} \\ B_{12} & B_{22} & B_{26} \\ B_{16} & B_{26} & B_{66} \end{bmatrix} \begin{bmatrix} \varepsilon_x^0 \\ \varepsilon_y^0 \\ \varepsilon_{xy}^0 \end{bmatrix} + \begin{bmatrix} D_{11} & D_{12} & D_{16} \\ D_{12} & D_{22} & D_{26} \\ D_{16} & D_{26} & D_{66} \end{bmatrix} \begin{bmatrix} \kappa_x \\ \kappa_y \\ \kappa_{xy} \end{bmatrix} \quad (17)$$

where ε and κ refer to strains and curvatures, [D] refers to bending stiffness matrix and [B] is the coupling stiffness matrix. Since the coupling matrix [B] is zero for symmetric laminates, bending moment vector becomes;

$$\begin{bmatrix} M_x \\ M_y \\ M_{xy} \end{bmatrix} = \begin{bmatrix} D_{11} & D_{12} & D_{16} \\ D_{12} & D_{22} & D_{26} \\ D_{16} & D_{26} & D_{66} \end{bmatrix} \begin{bmatrix} \kappa_x \\ \kappa_y \\ \kappa_{xy} \end{bmatrix} \tag{18}$$

where the inverse relation can be written as to give the effective flexural moduli in terms of the bending compliance matrix [D^*];

$$\begin{bmatrix} \kappa_x \\ \kappa_y \\ \kappa_{xy} \end{bmatrix} = \begin{bmatrix} D_{11}^* & D_{12}^* & D_{16}^* \\ D_{12}^* & D_{22}^* & D_{26}^* \\ D_{16}^* & D_{26}^* & D_{66}^* \end{bmatrix} \begin{bmatrix} M_x \\ M_y \\ M_{xy} \end{bmatrix} \tag{19}$$

When $M_y = 0$ and $M_{xy} = 0$, then Eq.19 becomes;

$$\kappa_x = D_{11}^* M_x \tag{20}$$

Finally, the effective flexural longitudinal modulus for symmetric laminates is determined based on CLT as follows

$$E_x^f = \frac{12M_x}{\kappa_x h^3} = \frac{12}{h^3 D_{11}^*} \tag{21}$$

Table 5.5 shows the longitudinal bending effects on shear strength. Comparison made for four specimens that have the same bottom adherends; only top adherends sequences and thicknesses are variable. The shear strength values are obtained from Eq. 2 which is;

$$\tau = \frac{P}{wl} \tag{2}$$

Table 5.5. *Longitudinal Bending Stiffness Effect on Shear Strength*

	Bottom adherend thickness [mm]/ Sequence	Top adherend thickness [mm]/ Sequence	D11*	Longitudinal bending stiffness [GPa] Ex=12/(D11*.t^3)	Max load [kN]	Shear Strength [MPa]
B5_T6_L40	1.6	5.552	0.001	55.19	10.55	10.45
	[45/0/45/0/45]	$[(45)_2/\underline{0}/\underline{135}/\underline{0}/\underline{45}/(\underline{0})_2/0/(\underline{0})_2/0/\underline{0}]_s$				
B5_T7_L40	1.6	4.624	0.002	48.94	13.13	13.02
	[45/0/45/0/45]	$[(45)_2/\underline{0}/\underline{135}/\underline{0}/\underline{45}/(\underline{0})_3/0/\underline{0}]_s$				
B5_T8_L40	1.6	3.152	0.008	46.34	10.65	10.67
	[45/0/45/0/45]	$[(45)_2/(\underline{0})_3/0/\underline{0}]_s$				
B5_T9_L40	1.6	2,504	0.022	35.39	8.38	8.33
	[45/0/45/0/45]	$[(45)_2/(\underline{0})_3/0/(\underline{0})_3/(45)_2]$				
B5_T10_L40	1.6	1.488	0.220	16.56	7.97	7.87
	[45/0/45/0/45]	$[(45)_2/\underline{0}]_s$				

5.1.4. Effects of Adhesive Joint Length and Thickness

As it is mentioned in literature [12], adhesive bond length and adherend thickness ratio (L/t) have an important effect on shear strength of joints. The results shown in Table 5.6 - Table 5.8 indicate that, the increase in adhesive bond length to adhesive thickness ratio results in an increase in the shear strength of the joint. For the specimens which bottom and top adherend thicknesses are different, comparisons are made on the specimens that have the same thickness for bottom adherends. Test results shows a coherency with Kutcha and Hofer study which is shown in Figure 5.18.

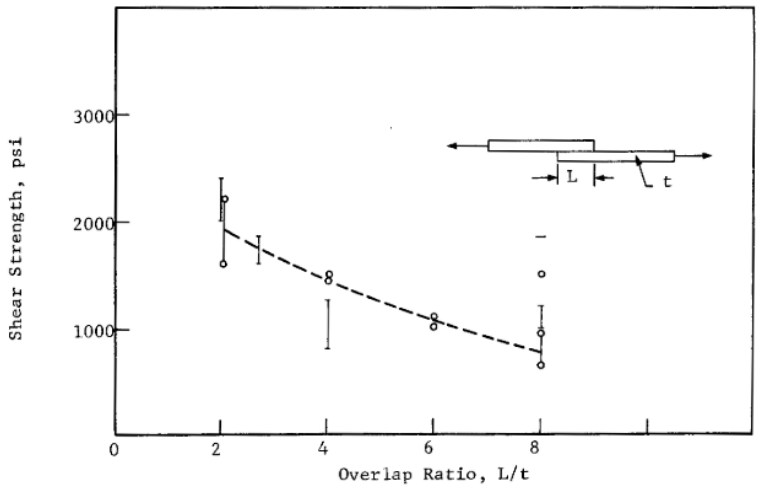

Figure 5.18. Shear strength to overlap ratio from Kutscaha and Hofer study[12]

Table 5.6. *L/t effect on Shear Strength of the joint for 1.6mm bottom adherend thickness*

	Bottom adherend thickness [mm]	Top adherend thickness [mm]	Joint Length [mm]	L/t	Max load [kN]	Shear Strength [MPa]
B4_T12_L26	1.6	5.552	26	4.68	12.19	18.14
B5_T6_L40	1.6	5.552	40	7.20	10.78	10.70
B5_T7_L40	1.6	4.624	40	8.65	12.66	12.57
B5_T8_L40	1.6	3.152	40	12.69	10.64	10.67
B5_T9_L40	1.6	2.504	40	15.97	8.38	8.33
B5_T10_L40	1.6	1.488	40	26.88	7.37	7.29

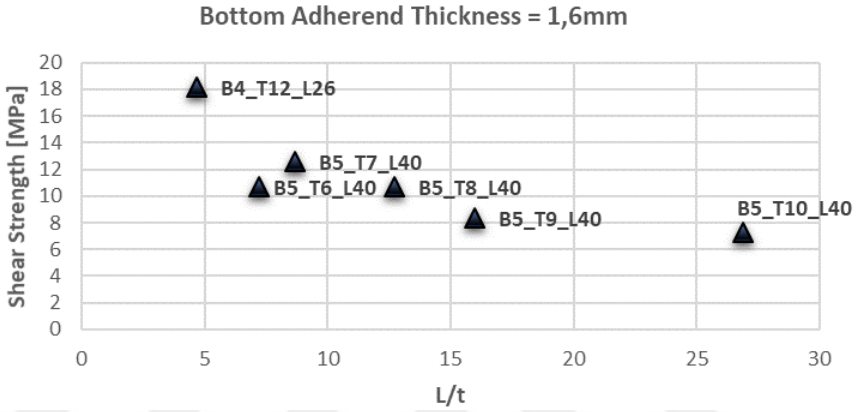

Figure 5.19. L/t effect on Shear Strength of the joint for 1.6mm bottom adherend thickness

Table 5.7. *L/t effect on Shear Strength of the joint for 2.44mm bottom adherend thickness*

	Bottom adherend thickness [mm]	Top adherend thickness [mm]	Joint Length [mm]	L/t	Max load [kN]	Shear Strength [MPa]
B2_T2_L28	2.44	8.864	28	3.16	15.95	22.35
B2_T3_L28	2.44	7.76	28	3.61	14.94	21.06
B3_T11_L28	2.44	5.552	28	5.04	11.30	16.06

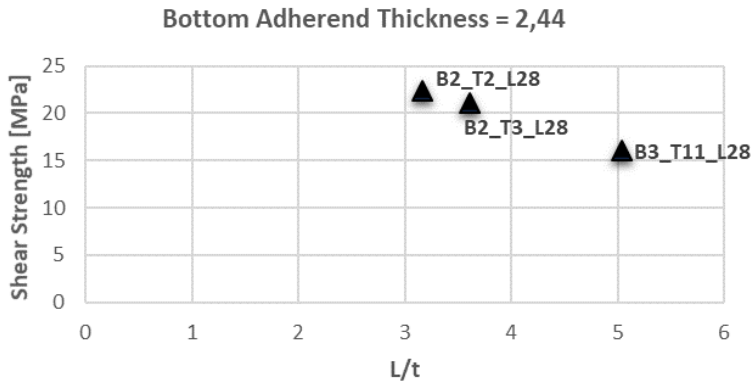

Figure 5.20. L/t effect on Shear Strength of the joint for 2.44mm bottom adherend thickness

Table 5.8. *L/t effect on Shear Strength of the joint for different joint length*

	Bottom adherend thickness [mm]	Top adherend thickness [mm]	Joint Length [mm]	L/t	Max load [kN]	Shear Strength [MPa]
B2_T3_L28	2.44	7.76	28	3.61	14.94	21.06
B3_T4_L40	2.44	7.76	40	5.15	14.47	14.32

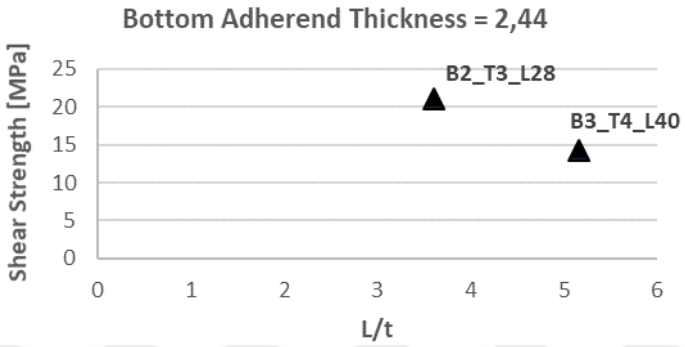

Figure 5.21. L/t effect on Shear Strength of the joint for different joint length

5.2. FEM Results

5.2.1. Investigation of Stress Distributions

Stress distributions in the SLJ specimens are presented in two sections. First an investigation for the stress distribution through the overlap length is carried on. Peel and shear stresses that concentrate on the adhesive are analyzed for three SLJ configurations which is given in Table 5.9. Second, the peel stress distribution in width direction for these three configurations is given. The analyses for the stress distribution in SLJ specimens with different configurations can help better understanding of failure behavior in such structures. At first, cohesive elements and failure criterion are not considered in the finite element model to obtain only the stress distribution. Moreover, solid element models are used since continuum shell elements does not provide stress values through the thickness direction.

Table 5.9. *Selected specimen configurations for stress analyses*

	Bottom adherend thickness [mm]/ Sequence	**Top adherend thickness [mm]/ Sequence**
B3_T4_L40	**2.44**	**7.76**
	[45/0/$(45)_2$/0/45**/0/45**]	[$(45)_2$/$(\underline{0})_2$/135/$(\underline{0})_2$/45/0/135/0/0/$(\underline{0})_2$/45/$(\underline{0})_2$/0/$\underline{0}]_s$
B5_T7_L40	**1.6**	**4.624**
	[45/0/45**/0/45**]	[$(45)_2$/0/135/0/45/$(\underline{0})_3$/0/$\underline{0}]_s$
B5_T10_L40	**1.6**	**1.488**
	[45/0/45**/0/45**]	[$(45)_2$/$\underline{0}]_s$

Stress distribution through the overlap length

Shear and peel stresses in SLJ specimens are investigated with a 3D finite element analysis at the mid-width of the adhesive across the bond-line of the bonded joint. At first, the stress distribution on top and bottom of the adhesive mid-width has been investigated. Later, comparisons are made on stress distributions among three SLJ configurations.

The peel stress distribution of the top and bottom edge of the adhesive through the overlap is given in Figure 5.22. It is seen to be much lower at the initiation of the overlap and reaches to a maximum value at the end due to the asymmetry of the joint. The high peel stress at the free edge of the interface is critical for evaluating the damage initiation at that location [25]. Due to the higher stress concentration at the bottom interface of the specimen, estimations can be made for the location of the crack initiation.

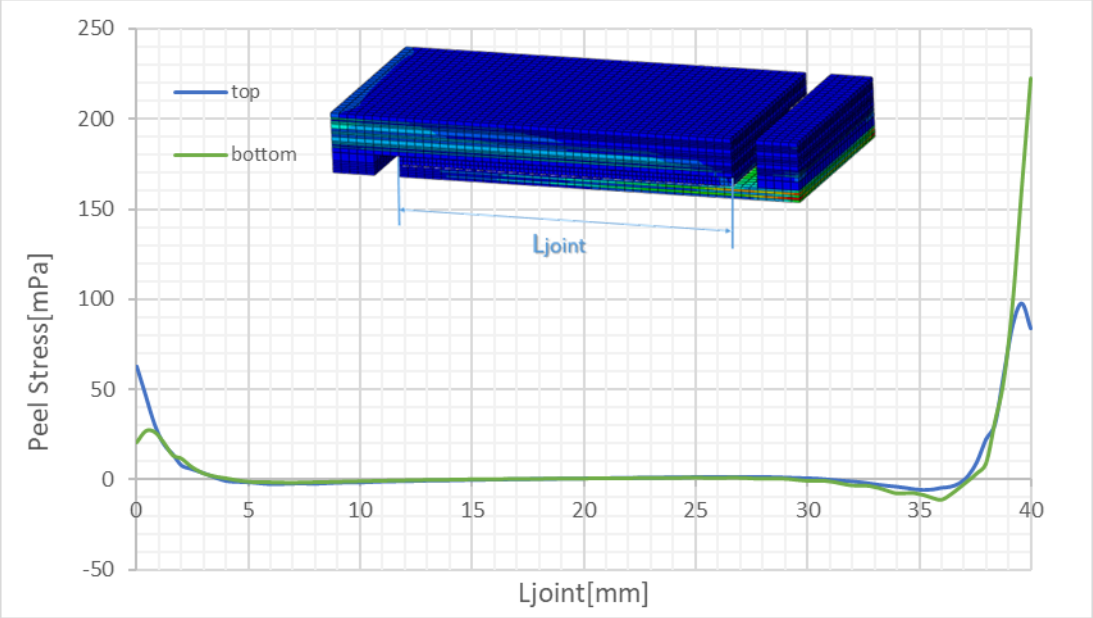

Figure 5.22. Peel stress on top and bottom of the adhesive

Comparisons of peel and shear stress distributions across the bond-line for three configurations are given in Figure 5.23 and Figure 5.24. The selected configurations are distinct from each other considering the increase of the asymmetry of the joint.

Peel and shear stresses show the maximum value to be at the left tip of the overlap. Peel stress increases toward its maximum at the edge because the free surface of the overlap which does not satisfy the traction free condition [43] and a singularity occurs at those edges. The peel stress then decreases suddenly to almost zero value through the inner side of the overlap, while shear stress concentrations gradually decrease but never approach to zero.

With the increase of the thickness of the top adherend, the stiffness difference between top and bottom adherend increases that leads to a higher bending moment. Different than the symmetric joints, it can be seen that peel and shear stress distributions on the right and left overlap edges are quite different. Left side of the overlap, shows higher peel and shear stresses. With the increase of asymmetry, the peel and shear stress that joint experiences increase significantly.

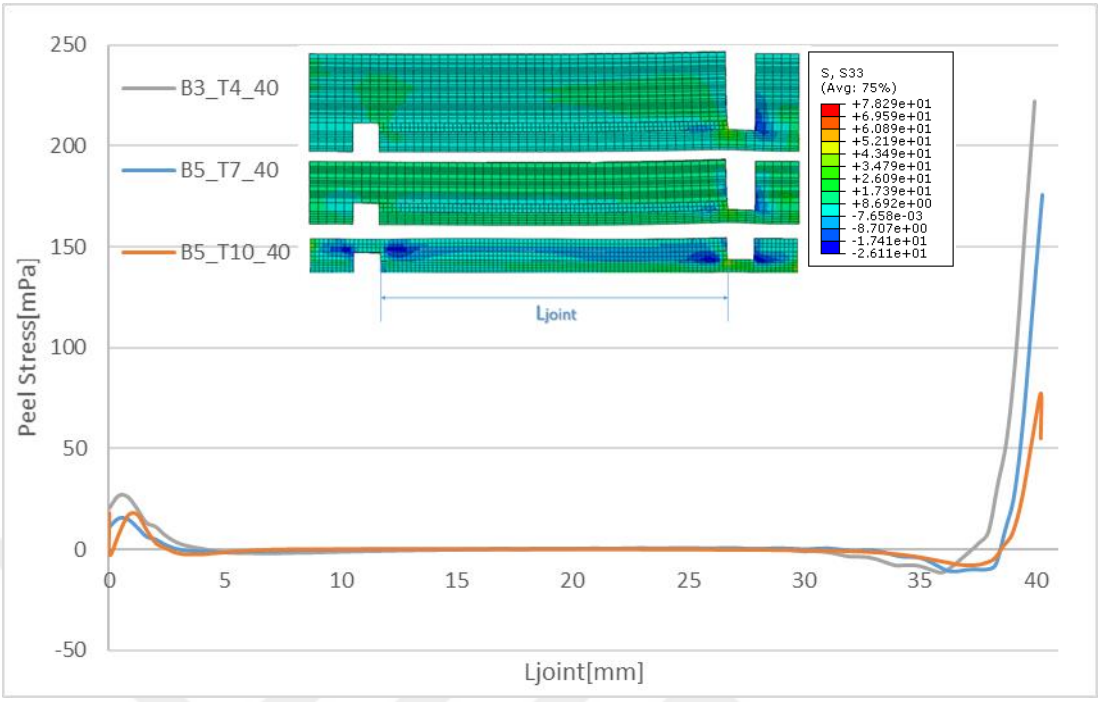

Figure 5.23. Comparison of Peel Stresses

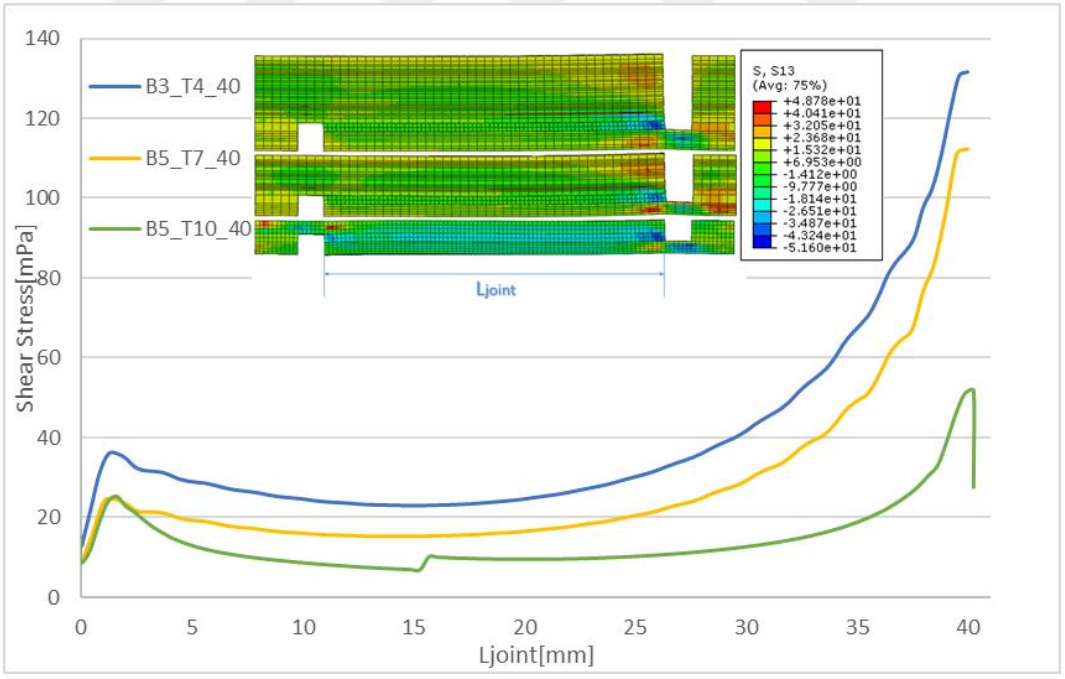

Figure 5.24. Comparison of Shear Stresses

Stress distribution in the width direction

Adhesive and adherend experience stresses exist also in width direction. However, they are relatively small when stresses in longitudinal direction is considered. Differently for the stress distribution through the overlap, the stress is lower at the free edges of the adhesive while maximum value is obtained in middle. On the other hand, the adhesive shear stress through the width shows an opposite behavior as the shear stress becomes maximum at the overlap edges and zero in the middle as shown in Figure 5.25.

Similar results are obtained in the finite element analysis. The peel and shear stress distributions of three test configurations in width direction can be seen in Figure 5.26 and Figure 5.27 respectively. With the increase in loading eccentricity, the peel stress rises due to increase in bending [25].

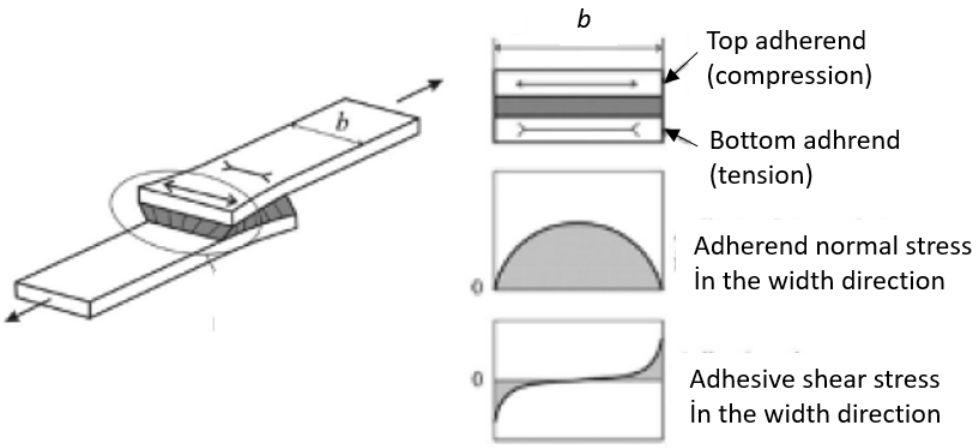

Figure 5.25. Peel Stress in Width Direction*[33]*

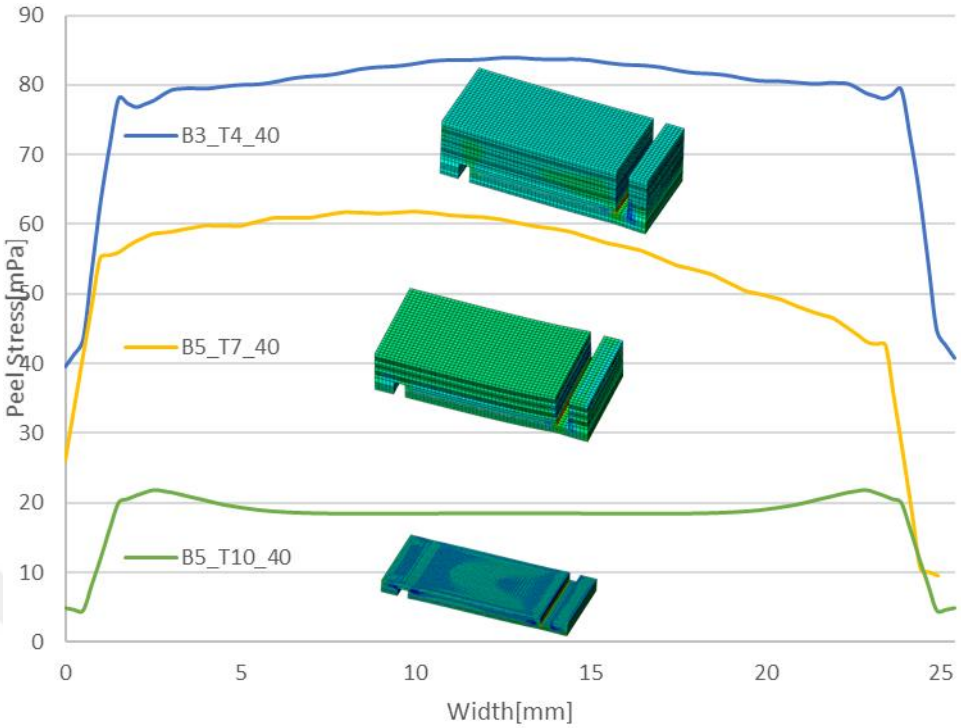

Figure 5.26. Peel Stress in Width Direction

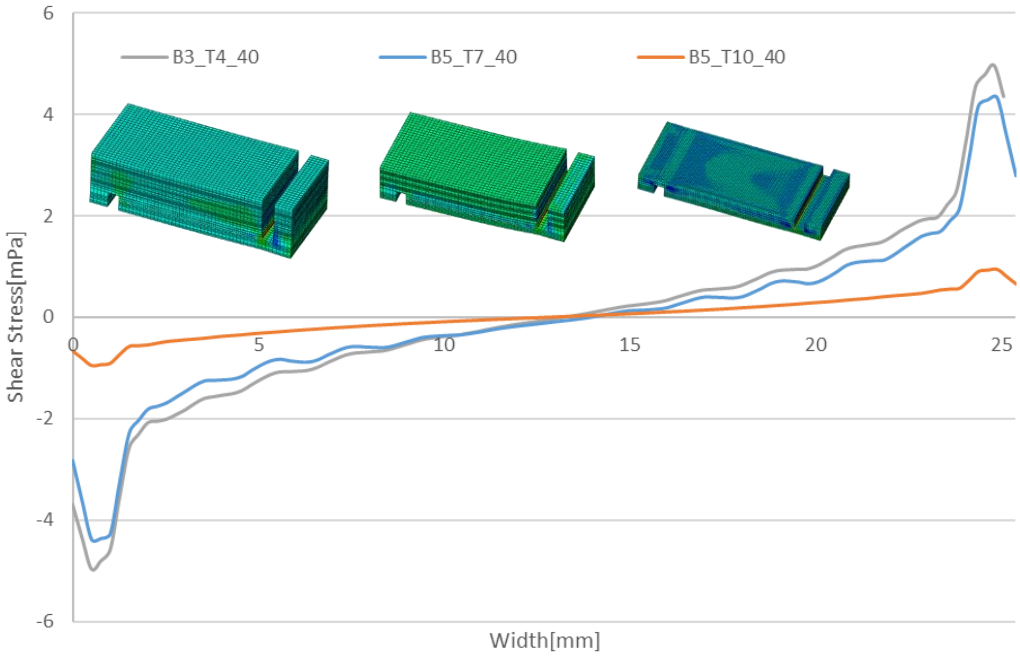

Figure 5.27. Shear Stress in Width Direction

5.2.2. Results in Cohesive Zone Model

A finite element model for adhesively bonded single lap joints is created to investigate the crack initiation and propagation. The cohesive zone method is used to simulate the crack at the interface between adhesive and adherends. Cohesive zone modelling and finite element analyses are performed in ABAQUS.

In contrast to the real life applications, a discrete adhesive is modelled, in other words, adhesive and interface models are only crated at the overlap as it can be seen in Figure 5.28. In consequence, stress singularities that take place at the point of the junction of the adherend and adhesive, translate to the opposite side of the interface. Even if crack initiation points are different in FEM and real life application, the crack propagation can be simulated properly with FEM.

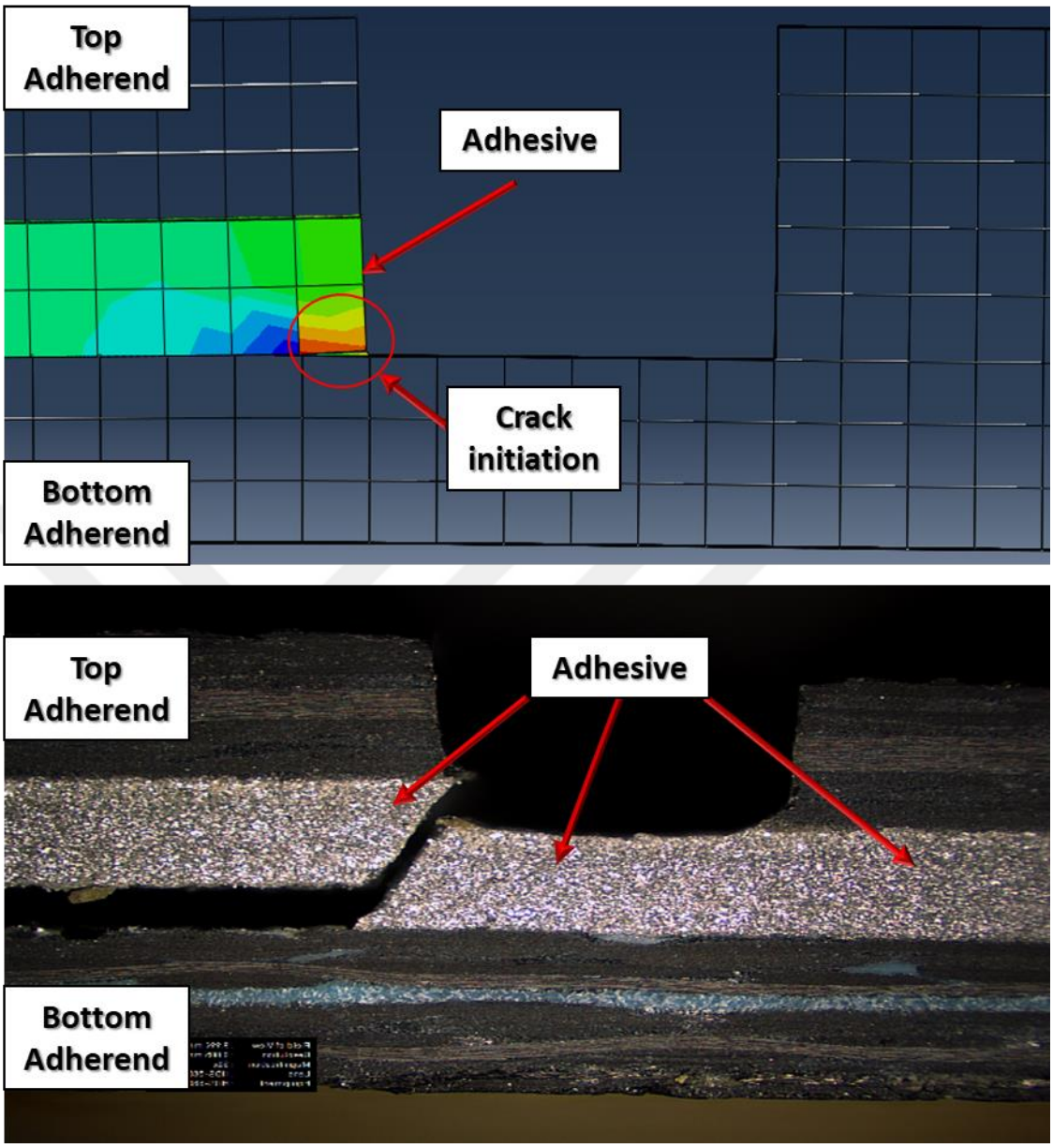

Figure 5.28. Discrete adhesive model

According to the analyses performed on Specimen *B5_T10_L40*, the initial crack is observed on the left side of the overlap as shown in Figure 5.29, where the joint experiences the maximum shear and peel stresses (Figure 5.30). This crack initiation point belongs to the thicker side of the adherend and this result is compatible with the high speed video camera results as it can be seen in Figure 5.15.

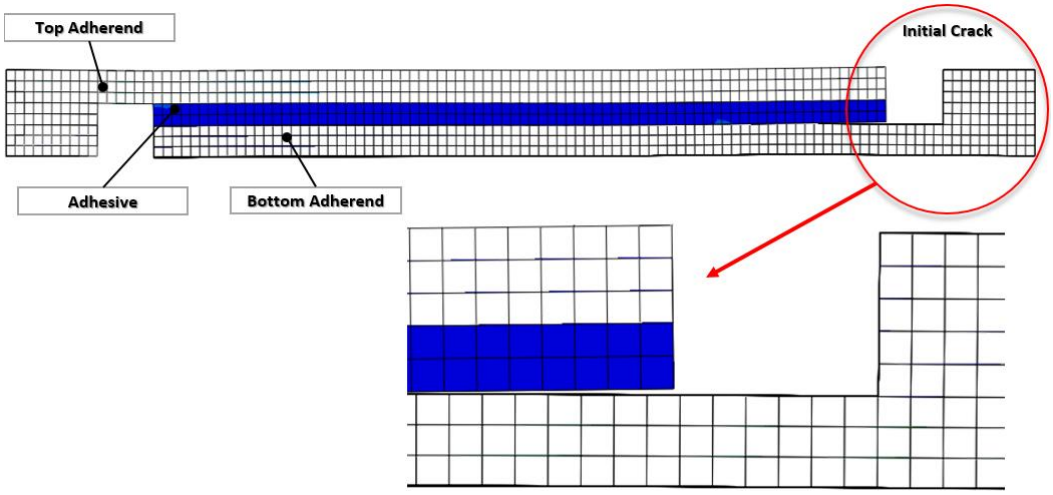

Figure 5.29. Interface crack initiation in Specimen B5_T10_L40

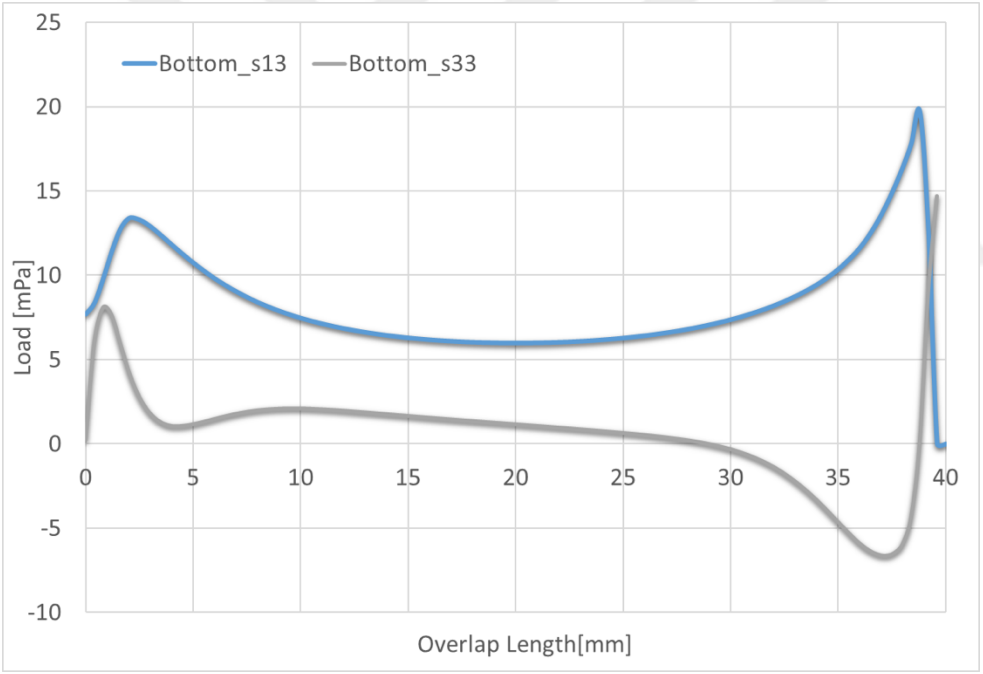

Figure 5.30. Specimen B5_T10_L40: Bottom interface stress distribution along overlap

Crack propagation also investigated step by step for the same configuration to compare the results with the SLJ test results. When the stress state in cohesive elements meet the failure criteria, the element deletion takes place in the analysis. In

Figure 5.33, intermediate steps in the analyses are given to show element deletion, namely the crack propagation. As it is represented before, the crack initiates from the left side of the overlap where the thicker adherend ends. Afterwards the crack propagates along the overlap at the interface between adhesive and bottom adherend. When the first initiated crack pass beyond the mid of the overlap, a second crack initiates from the opposite interface which is in between adhesive and the top adherend.

According to the SLJ test results, one can make conclusions for the failure behavior in SLJ specimens. In Figure 5.31, a similar behavior can be observed in finite analysis since the interface crack occurs at both sides of the overlap. Cohesive crack takes place in real life applications distinctly in FEM since ABAQUS material models are used to model adhesive and interface. To simulate cohesive crack, a new material model should be developed.

Figure 5.31. Microscopic examination of Specimen B5_T10_L40 SLJ

Load displacement result of CZM is compared with the mechanical test results on 8 specimens and distinctive linear behavior is obtained in Figure 5.32. Besides, finite element analyses that have performed without cohesive elements are not coherent with the test results as well. It can be explained with the discrete model usage in FEM application to overcome the limitations in material model of ABAQUS, the stiffness of the joint may change comparing to real life application due. Performing such comparison is only logical with the creation of new FEM that have full length adhesive and with the new material model in ABAQUS that has the capability of crack propagation within different materials.

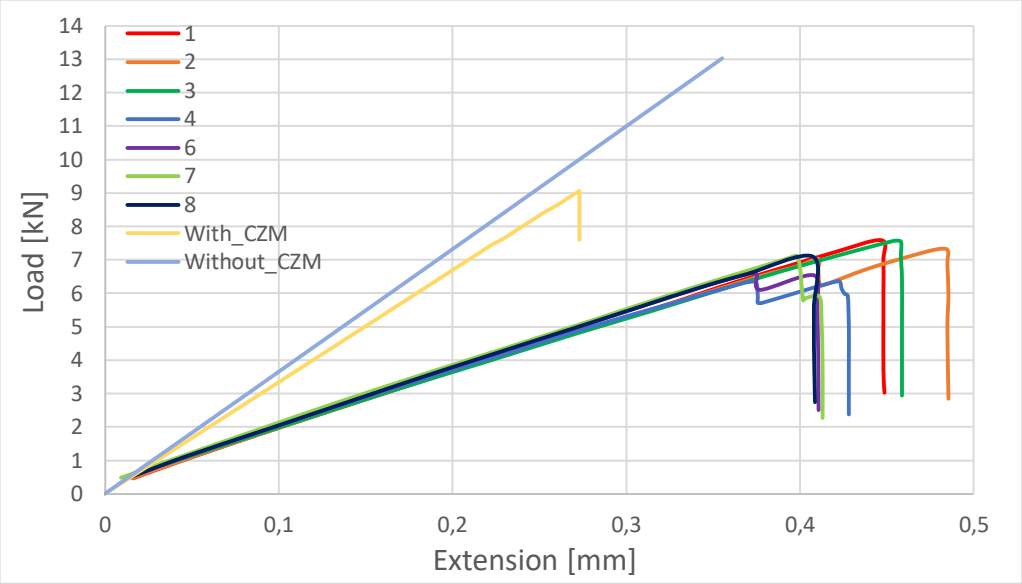

Figure 5.32. Load-Displacement comparison of B5_T10_L40 SLJ

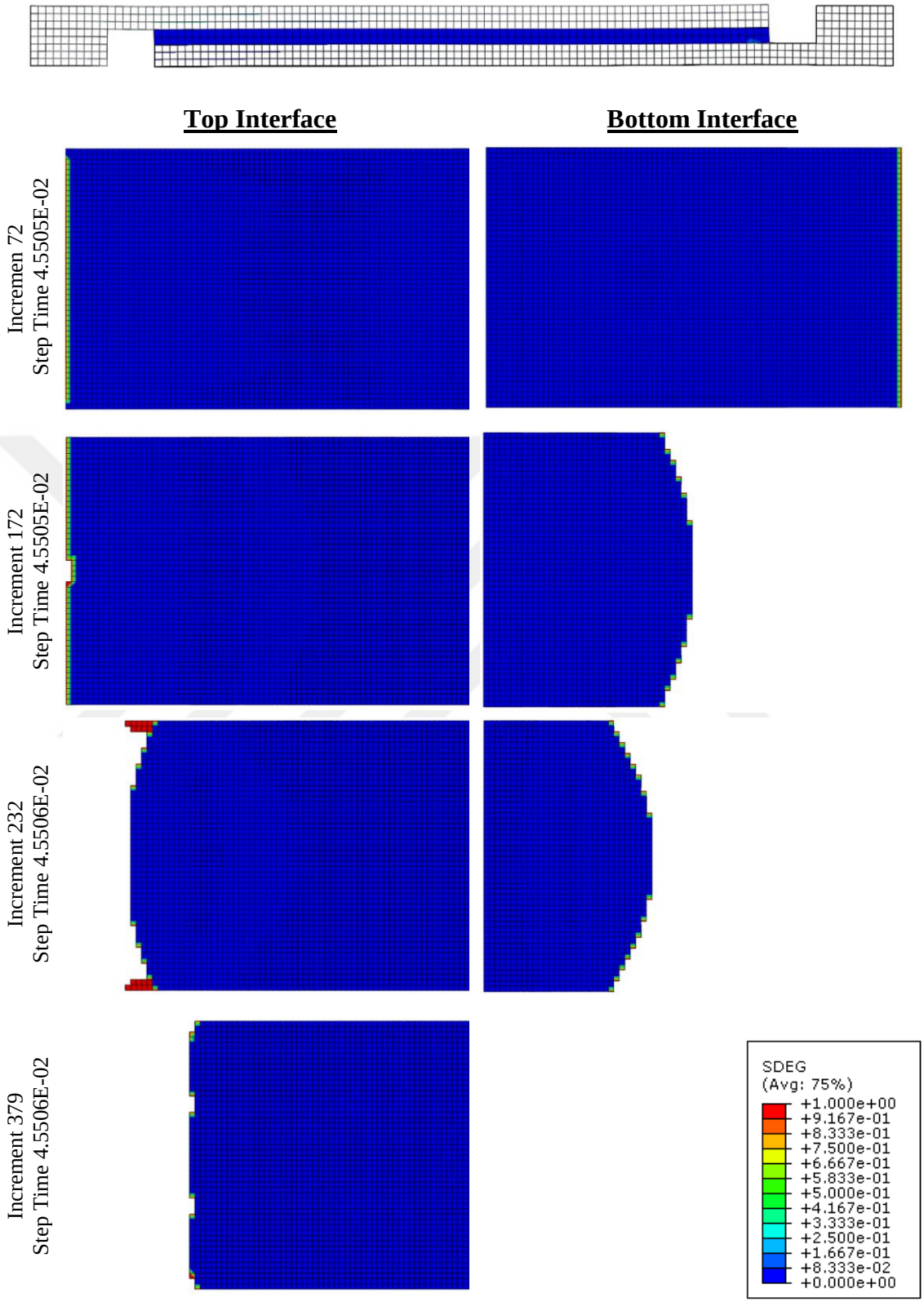

Figure 5.33. Step by step crack propagation

To make a generalization for the failure behavior, finite element analyses performed with SLJ specimens have the same overlap length and bottom adherend sequence, but have different top adherend thickness (Figure 34). Results of FEM model for four specimens with the same displacement are represented and it can be clearly seen that, the crack initiates from the thicker side of the joint for all specimens. In specimens that have thinner top adherends, a second crack initiation is observed from the opposite side of the overlap, while there is no second crack initiation at the specimens with thicker adherends. It can be explained with the fact that thinner adherends experience a higher bending moment due to their low bending stiffness.

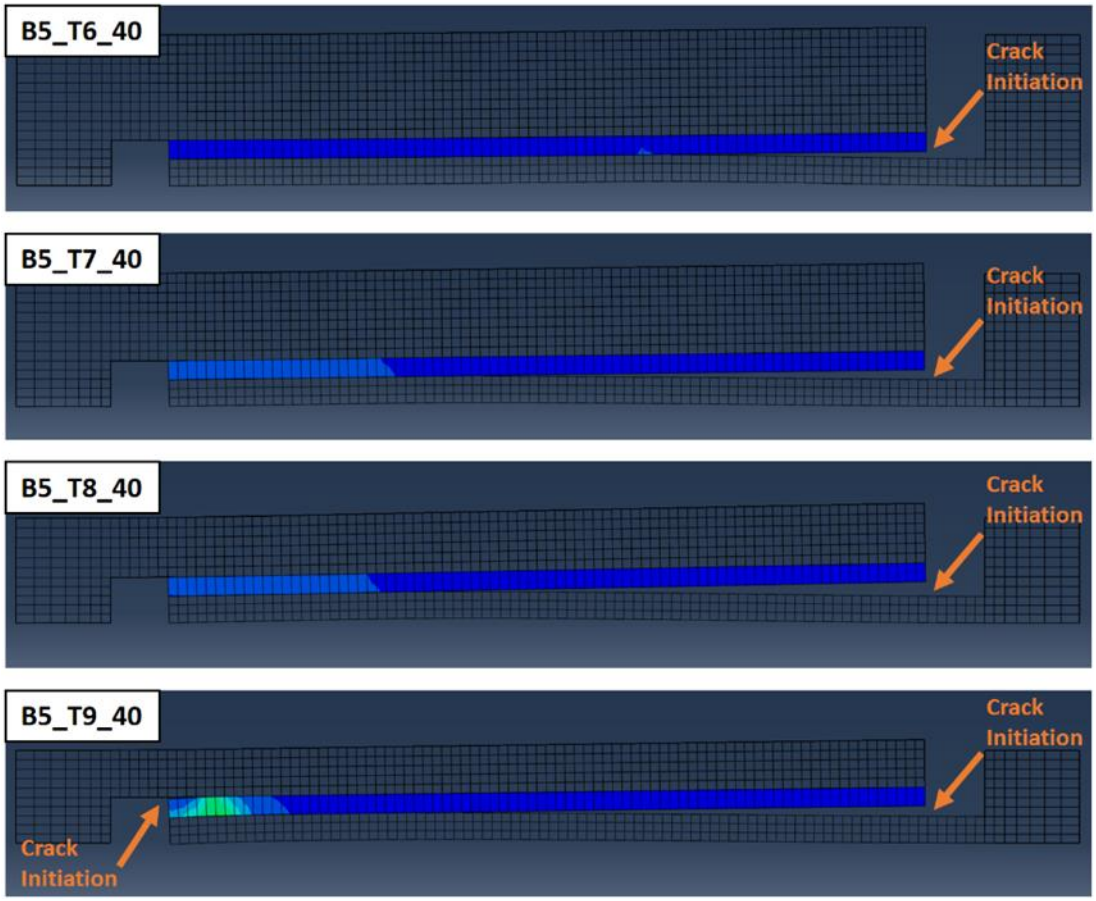

Figure 5.34. Failure behavior comparison in FEM

CHAPTER 6

CONCLUSION

6.1. Summary

The adhesive bonding started to become one of the frequently preferred methods in recent years due to their substantial advantages. Increase in the usage of composites in aerospace industry boosted the role of the adhesive bonding in primary and secondary structures. Despite various advantages, the maturity of adhesive bonding studies in terms of the estimation of failure behavior, material models have not yet reached to the level of mechanical fastening. In the scope of this study, the failure behavior of adhesively bonded joints are investigated.

The failure mechanism of adhesively bonded joints are investigated with single lap joint specimens. Adherends which are created from composite plies with various thicknesses and stacking sequences has been used in the study to analyze the effect of thickness and stiffness of the adherends to the failure behavior of the adhesively bonded joints. Furthermore, effect of overlap length also taken into consideration.

A mechanical test program is conducted for single lap joint specimens. Different number of plies and/or sequences are defined for composite adherends. 12 different sequences for top adherends and 6 different sequences for bottom ones are determined. Laminates are manufactured with fabric and UD plies using co-bonding and co-curing methods. The manufactured adherends are bonded together with the secondary bonding method to finalize the single lap joint geometry.

Single lap joint specimens are tested in universal test machine under tension and specimens are loaded until 40% drop in load is observed. Each test for the same configuration is repeated at least six times to provide reliability of results. Load-displacement curves are obtained in the test program.

Effects of the bending stiffness are investigated with the comparison of 4 selected specimen configurations which have the same bottom adherend sequence and joint length. Composite sequence of the top adherend is defined as the only variable and longitudinal bending stiffness values are calculated for each configuration by using CLT. Results showed that, a higher shear strength is obtained with the increase in bending stiffness. In Kupksi study, it is explained that the increase in bending stiffness leads to a decrease in peel stresses which in turn increases the joint strength [10].

In the next step, effects of adhesive joint length to thickness ratio is investigated. 6 different configurations that have the similar bottom adherends are compared. Higher shear strength results are obtained with the decrease in *L/t* ratio. The results are correlated with the results obtained from Kutscha and Hofer [12].

Microscopic examination has been performed on selected test configurations in order to investigate the failure modes. With the help of microscopic examination, crack locations, crack shapes and crack jumps are investigated. An adhesive failure is observed in all specimens with the separation at the interface between adhesive and adherends. But in some specimens, cracks within adhesive material is also detected that is called as cohesive failure in literature. However, if only the main reason of the failure is taken into account, it can be said that the adhesive failure mode is effective in all specimens since the cohesive failure takes place after the crack initiation at the interface.

The end of the overlaps experiences the stress singularity at the interface corner where the crack initiation is expected to be observed. In the microscopic examination, the crack initiates at the corner of adhesive and adherend where high stresses exist and it propagates with an angle toward the opposite interface which is in compression. This situation is also observed in Karachalios' paper [10] as the adhesive materials are stronger in compression than they are in tension. The angular crack propagation shows the bending moment effect in SLJ specimens.

Due to the difficulty in predicting the crack initiation and propagation in already cracked specimens, a SLJ test repeated with a high speed video camera. By this way, the crack initiation area is detected and the results are interpreted along with considerations of literature.

In contrast to the conclusion in Kutscha and Hofer [12] as the crack initiates from the thicker part of the joint for unbalanced configuration, the crack initiation is observed at the overlap at the thicker side of the joint. To make final conclusion on the crack initiation, finite element analyses are performed in advance.

A finite element model of adhesively bonded single lap joints specimens are created using ABAQUS. A three dimensional model is used to investigate out-of-plane stresses due to the eccentricity of the loading on joint that causes a bending moment.

Stress distribution created along the overlap and width is used to explain the failure behavior in SLJ joints. Higher peel and shear stress concentrations obtained at the thicker side of the overlap end where lower stresses obtained on the opposite side due to the eccentricity in the joint. With the increase in the difference between adherend stiffnesses, higher peel and shear stresses are observed. Similar results are obtained for the stress distribution in the width direction. With the aim of modelling the interface crack in SLJ specimens, cohesive zone model is used for interface elements between adherends and bulk adhesive. Cohesive elements are modelled with a finite thickness and top and bottom nodes of the elements are translated to create a zero thickness element.

There is no solution in ABAQUS for failure propagation between different materials. For that reason, a discrete adhesive model is constructed instead of a full length adhesive as it is in the real life applications. In consequence, the crack initiation directly transferred to the interface which is in compression.

Similar results are obtained with the previous estimations according to the results in stress distribution analyses and the results are taken from high speed camera test. The crack initiation is observed at the thicker adherend side of the overlap. Moreover,

crack from both sides of the interface is detected for the joints that have lower stiffness. It is shown that the finite element results are in good correlation with the real life applications.

6.2. Concluding remarks

With the aim of comprehension of the failure mechanisms of bonded single lap joints, a study whose main structure consists of mechanical tests and finite element analyses is performed. In contrast to most of the studies in the literature, asymmetric joint and composite adherends are used here.

Test results show that the crack initiation takes place at the area under tension which is the junction point of adhesive and adherend. Due to the asymmetry of the joint, the crack initiation is observed at the side of the overlap where the thicker adherend ends. Then, the crack propagates through the adhesive until it reaches the opposite adherend. Further crack propagation takes place at the interface between adherend and adhesive which is called as the adhesive failure in bonded joints.

The test results are supported by finite element analyses in general. Shear and peel stress distributions for asymmetric joints are determined. Higher peel and shear stress obtained from the side of the overlap where thicker adherend ends and this causes a crack initiation at the joint. With the increase in asymmetry at the top and bottom adherend, higher peel and shear stresses are observed within the joint.

Although mechanical tests and elastic analyses are useful to make decisions about crack initiation, they are insufficient to determine the crack propagation in joints that have multiple cracks in the overlap area. By using cohesive zone elements, both the crack initiation and propagation are determined properly. It is represented that in thinner adherends, right after from the first crack initiation, a second crack is observed from the opposite overlap edge which can be explained through the fact that thinner adherends experience a higher bending moment due to their low bending stiffness.

6.3. Future Studies

The following studies are suggested as the future work to extend the understanding of the failure behavior of adhesively bonded lap joints;

- A more extensive test program can be designed to investigate the effect of composite stacking sequence in specimens with constant thickness
- A brittle adhesive material model can be created to simulate the cohesive crack in the adhesive bulk material

REFERENCES

[1] R. L. Bowen, F. C. Eichmiller, W. a Marjenhoff, and N. W. Rupp, "Adhesive bonding of composites.," J. Am. Coll. Dent., vol. 56, no. 2, pp. 10–13, 1989.

[2] Banea, M. D., & da Silva, L. F. (2009). Adhesively bonded joints in composite materials: an overview. *Proceedings of the Institution of Mechanical Engineers, Part L: Journal of Materials: Design and Applications*, *223*(1), 1-18.

[3] A. P. Vassilopoulos, Fatigue and Fracture of Adhesively-bonded Composite Joints Behaviour , Simulation and Modelling. 2015.

[4] Guan, Z. D., Wu, A. G., & Jin, W. A. N. G. (2004). Study on ASTM shear-loaded adhesive lap joints. Chinese Journal of Aeronautics, 17(2), 79-86.

[5] D. C. Noorman, "Cohesive Zone Modelling in Adhesively Bonded Joints," Thesis, p. 172, 2014.

[6] L. F. M. da Silva and R. D. S. G. Campilho, Advances in Numerical Modeling of Adhesive Joints. 2012.

[7] L. F. M. Silva and R. F. T. Lima, "Development of a Computer Program for the Design of Adhesive Joints," no. October 2014, pp. 37–41.

[8] L. F. M. Silva, R. F. T. Lima, R. M. S. Teixeira, and A. Puga, "Closed-form solutions for adhesively bonded joints," Reports Proj. Dev. Softw. Des. Adhes. joints, no. 1938, pp. 1–32, 2008.

[9] Davis, M. J., & Bond, D. A. (1999, July). The importance of failure mode identification in adhesive bonded aircraft structures and repairs. In International Conference on Composite Materials(Vol. 12, pp. 5-9

[10] Karachalios, E. F., Adams, R. D., & da Silva, L. F. (2013). The behaviour of single lap joints under bending loading. Journal of Adhesion Science and Technology, 27(16), 1811-1827.]

[11] J. Kupski, S. T. De Freitas, D. Zarouchas, P. P. Camanho, and R. Benedictus, "Composite layup effect on the failure mechanism of single lap bonded joints," Compos. Struct., vol. 217, no. December 2018, pp. 14–26, 2019.

[12] Kutscha, D., & Hofer Jr, K. E. (1969). FEASIBILITY OF JOINING ADVANCED COMPOSITE FLIGHT VEHICLE STRUCTURES. IIT RESEARCH INST CHICAGO ILL MECHANICS OF MATERIALS RESEARCH DIV.

[13] Hart-Smith, L. J. (1985). Designing to minimize peel stresses in adhesive-

bonded joints. In Delamination and debonding of materials. ASTM International.

[14] Reis, P. N., Ferreira, J. A. M., & Antunes, F. (2011). Effect of adherend's rigidity on the shear strength of single lap adhesive joints. International Journal of Adhesion and Adhesives, 31(4), 193-201.

[15] D. S. Dugdale, "Yielding of steel sheets containing slits," J. Mech. Phys. Solids, vol. 8, no. 2, pp. 100–104, May 1960.

[16] Camanho, P. P., Davila, C. G., & De Moura, M. F. (2003). Numerical simulation of mixed-mode progressive delamination in composite materials. *Journal of composite materials*, *37*(16), 1415-1438.

[17] Zou, Z., Reid, S. R., Li, S., & Soden, P. D. (2002). Modelling interlaminar and intralaminar damage in filament-wound pipes under quasi-static indentation. *Journal of composite materials*, *36*(4), 477-499.

[18] Turon Travesa, Albert. Simulation of delamination in composites under quasi-static and fatigue loading using cohesive zone models. Universitat de Girona, 2006.

[19] G. Alfano and M. A. Crisfield, "Finite element interface models for the delamination analysis of laminated composites: Mechanical and computational issues," Int. J. Numer. Methods Eng., vol. 50, no. 7, pp. 1701–1736, 2001.

[20] Pardoen, T., Ferracin, T., Landis, C. M., & Delannay, F. (2005). Constraint effects in adhesive joint fracture. *Journal of the Mechanics and Physics of Solids*, *53*(9), 1951-1983.

[21] Kafkalidis, M. S., & Thouless, M. D. (2002). The effects of geometry and material properties on the fracture of single lap-shear joints. *International Journal of Solids and Structures*, *39*(17), 4367-4383.

[22] Stuparu, F. A., Apostol, D. A., Constantinescu, D. M., Picu, C. R., Sandu, M., & Sorohan, S. (2016). Cohesive and XFEM evaluation of adhesive failure for dissimilar single-lap joints. *Procedia Structural Integrity*, *2*, 316-325.

[23] Abaris, M. J. H. Adhesive Bonding of Composites": lecture notes. Training Inc.

[24] Tsai, M. Y., & Morton, J. (1994). An evaluation of analytical and numerical solutions to the single-lap joint. International Journal of Solids and Structures, 31(18), 2537-2563.

[25] C. Yang and S. Pang, "Stress-Strain Analysis of Single-Lap Composite Joints Under Tension," 2016.

[26] T. Loading and T. Loading, "Standard Practice for Classifying Failure Modes in Fiber-Reinforced-Plastic (FRP)," vol. i, no. Reapproved, pp. 4–6, 2005.

[27] Heslehurst, R. B. (2013). Design and analysis of structural joints with composite materials. DEStech Publications, Inc.

[28] ASTM International. (2010). Standard test method for apparent shear strength of single-lap-joint adhesively bonded metal specimens by tension loading (metal-to-metal). ASTM international.

[29] Standard, A. S. T. M. (2007). Standard test method for strength properties of adhesives in shear by tension loading of single-lap-joint laminated assemblies.

[30] ASTM, D. (2001). 5656,'Standard test method for thick-adherend metal lap-shear joints for determination of the stress-strain behavior of adhesives in shear by tension loading'. Annual Book of ASTM Standards, 15, 473-478.

[31] McCann, S. M. (2015). Numerical analysis of adhesively bonded single lap joints under high speed tensile loading (Doctoral dissertation, Wichita State University).

[32] Xu, X. P., & Needleman, A. (1994). Numerical simulations of fast crack growth in brittle solids. Journal of the Mechanics and Physics of Solids, 42(9), 1397-1434.

[33] R. D. S. G. Campilho, Strength Prediction of Adhesively-Bonded Joints, vol. 23, no. October 2002. 2017.

[34] H. Khoramishad, A. D. Crocombe, K. B. Katnam, and I. A. Ashcroft, "Predicting fatigue damage in adhesively bonded joints using a cohesive zone model," Int. J. Fatigue, vol. 32, no. 7, pp. 1146–1158, 2010.

[35] G. Perillo, N. P. Vedvik, and A. T. Echtermeyer, "Numerical analyses of low velocity impacts on composite . Advanced modelling techniques .," pp. 1–16, 2012.

[36] Abaqus Documentation (2009) Dassault Systèmes, Vélizy-Villacoublay

[37] Turon, A., Davila, C. G., Camanho, P. P., & Costa, J. (2007). An engineering solution for mesh size effects in the simulation of delamination using cohesive zone models. *Engineering fracture mechanics*, *74*(10), 1665-1682

[38] Yang, Q., & Cox, B. (2005). Cohesive models for damage evolution in l aminated composites. *International Journal of Fracture*, *133*(2), 107-137.

[39] Benzeggagh, M. L., & Kenane, M. J. C. S. (1996). Measurement of mixed-mode delamination fracture toughness of unidirectional glass/epoxy composites with mixed-mode bending apparatus. *Composites science and technology*, *56*(4), 439-449.

[40] Gonçalves, J. P. M., De Moura, M. F. S. F., De Castro, P. M. S. T., & Marques, A. T. (2000). Interface element including point-to-surface constraints for three-

dimensional problems with damage propagation. *Engineering Computations*, *17*(1), 28-47.

[41] Tvergaard, V., & Hutchinson, J. W. (1996). On the toughness of ductile adhesive joints. *Journal of the Mechanics and Physics of Solids*, *44*(5), 789-800.

[42] Alfano, G. (2006). On the influence of the shape of the interface law on the application of cohesive-zone models. *Composites Science and Technology*, *66*(6), 723-730.

[43] Chen, F., & Qiao, P. (2012). On the intralaminar and interlaminar stress analysis of adhesive joints in plated beams. International Journal of Adhesion and Adhesives, 36, 44-55.

[44] Goland, M., and E. Reissner. "J. of Applied Mechanics." *Trans ASME* 66 (1944): A17-27.

APPENDICES

A. Load Displacement Curves of SLJ Specimens

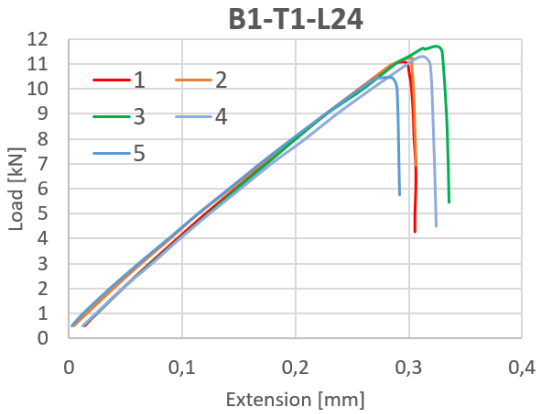

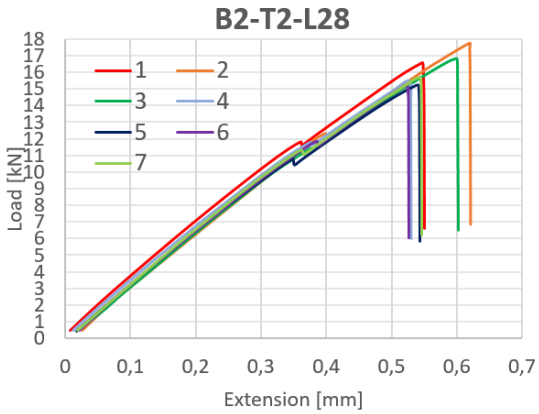

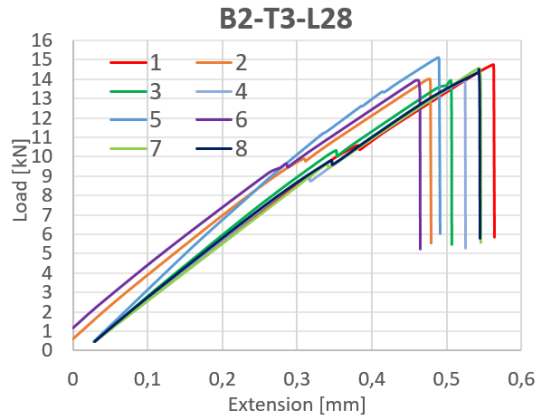

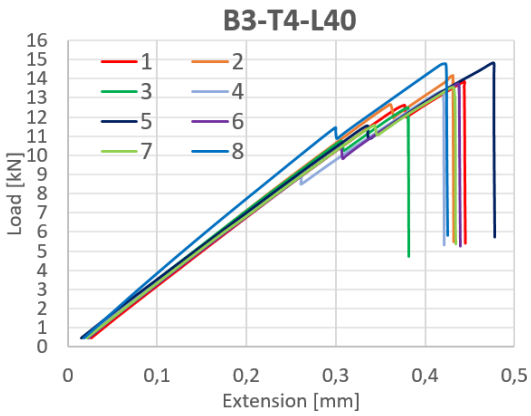

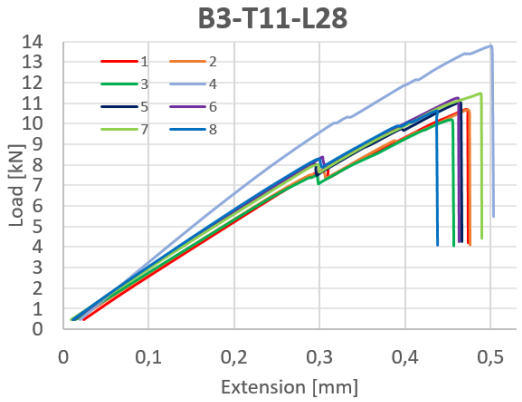

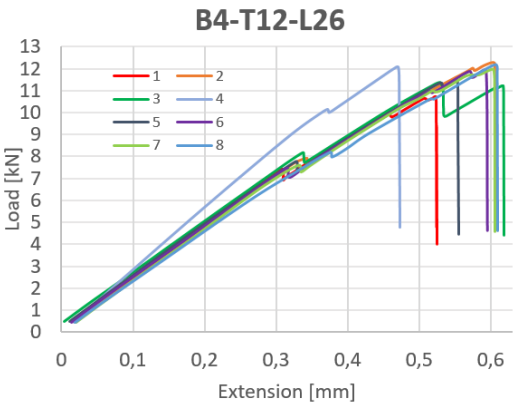

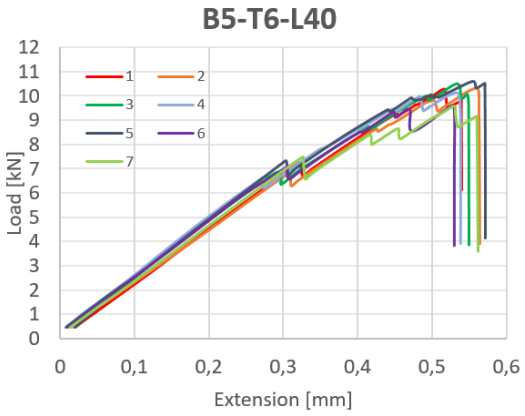
B5-T6-L40
Load [kN]
Extension [mm]
1
2
3
4
5
6
7

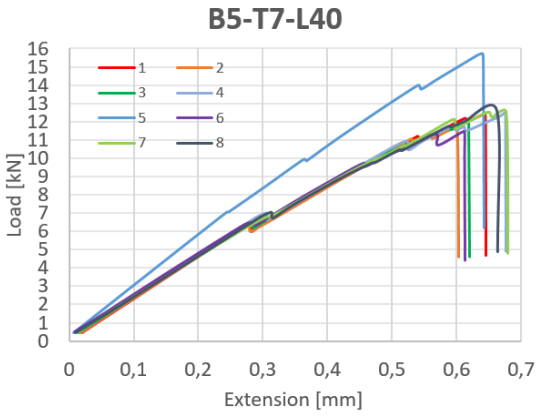
B5-T7-L40
Load [kN]
Extension [mm]
1
2
3
4
5
6
7
8

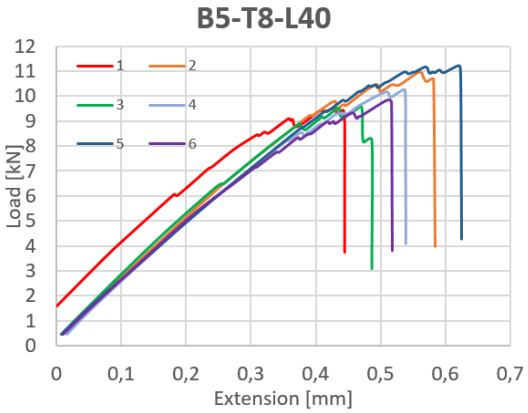
B5-T8-L40
Load [kN]
Extension [mm]
1
2
3
4
5
6

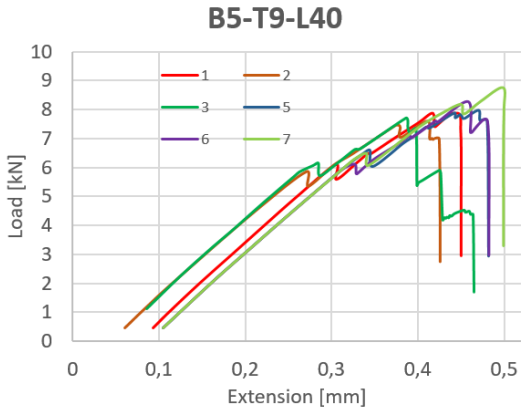
B5-T9-L40
Load [kN]
Extension [mm]
1
2
3
5
6
7

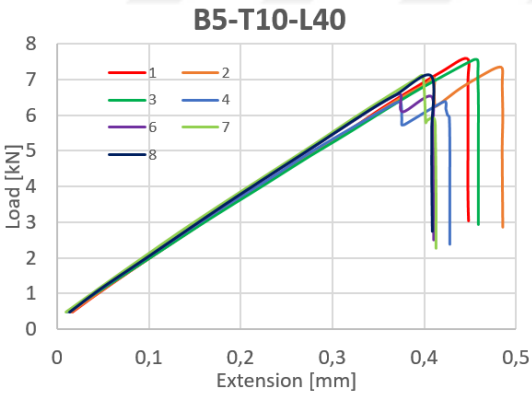
B5-T10-L40
Load [kN]
Extension [mm]
1
2
3
4
6
7
8

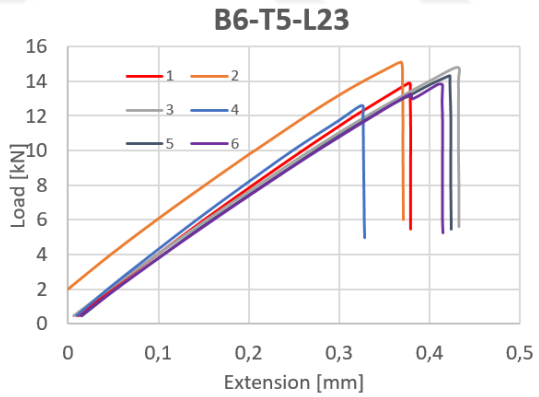
B6-T5-L23
Load [kN]
Extension [mm]
1
2
3
4
5
6

B. Microscopic Examination of SLJ Specimens

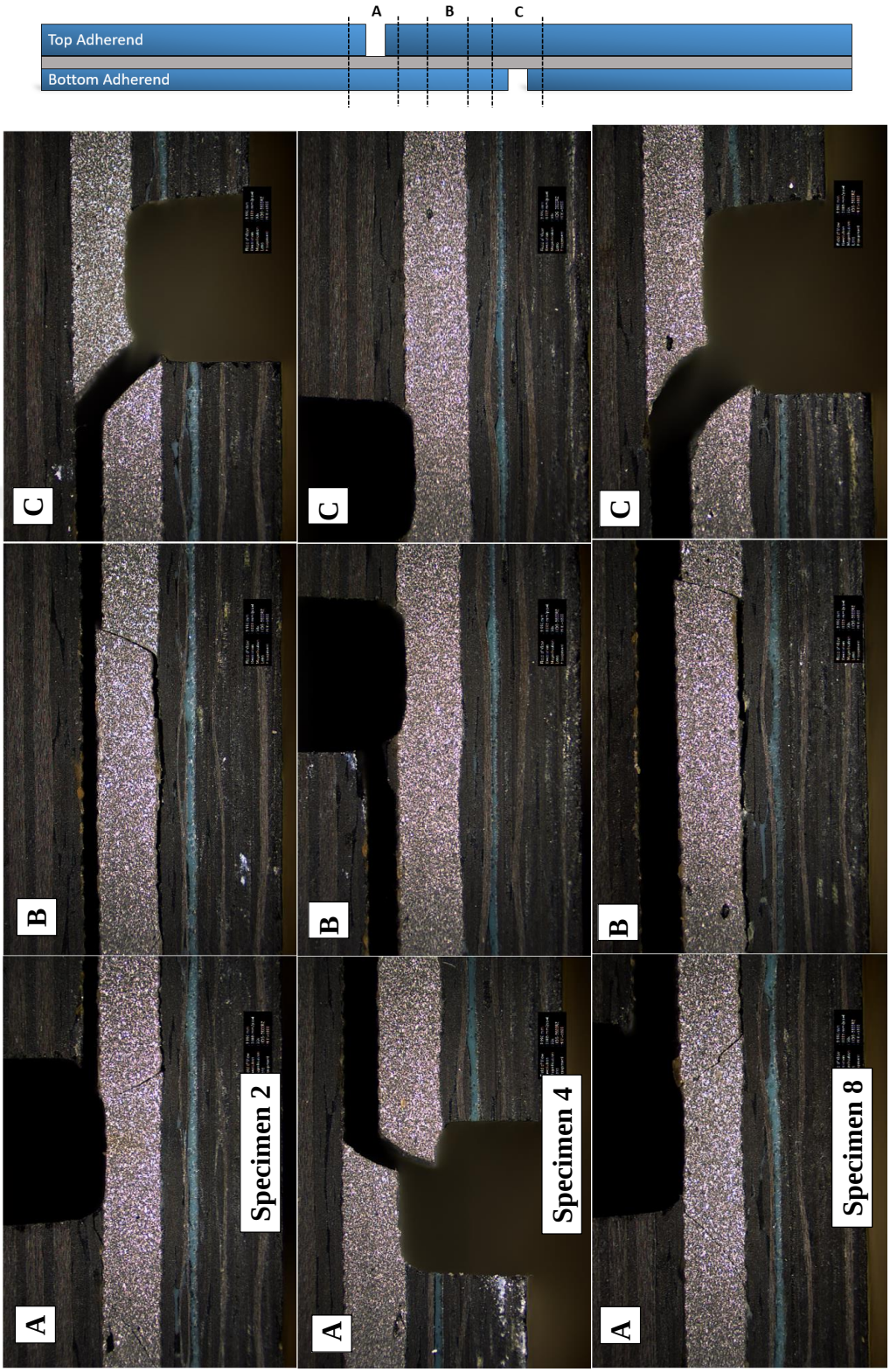

Figure B.1. Microscopic Examination of B2_T2_28 Specimen

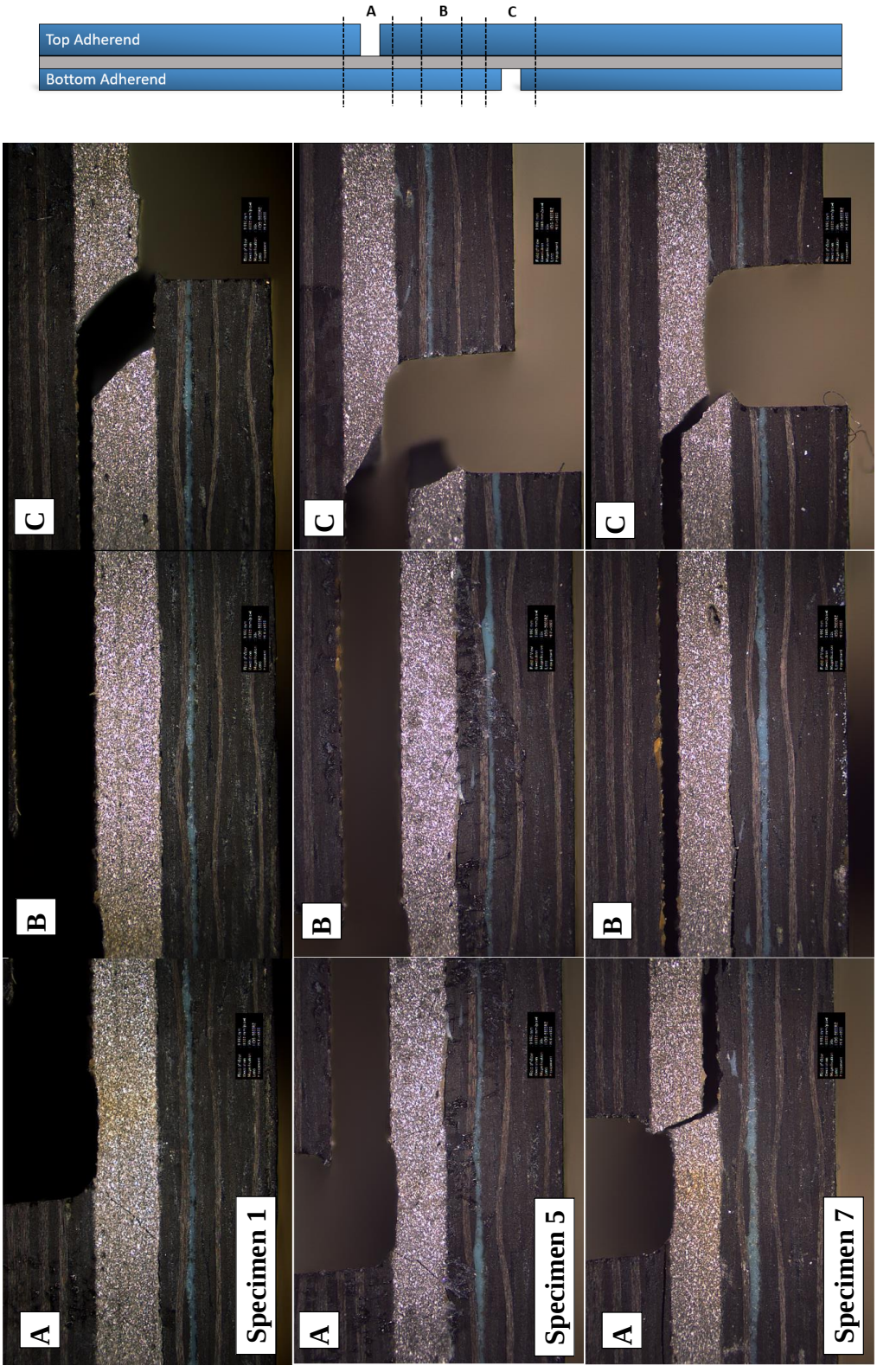

Figure B.2. Microscopic Examination of B3_T11_28 Specimen

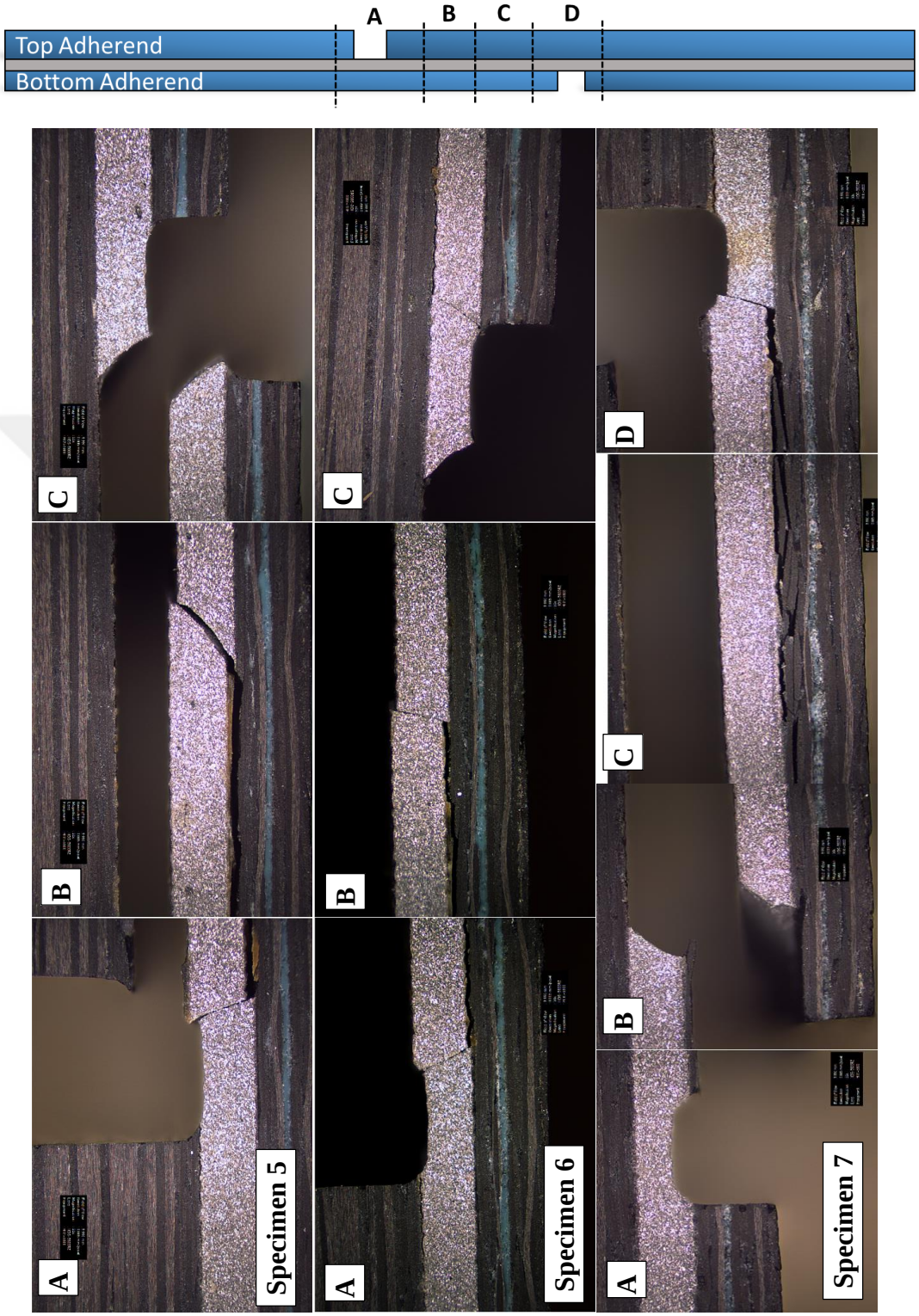

Figure B.3. Microscopic Examination of B5_T6_40 Specimen

Figure B.4. Microscopic Examination of B5_T10_40 Specimen

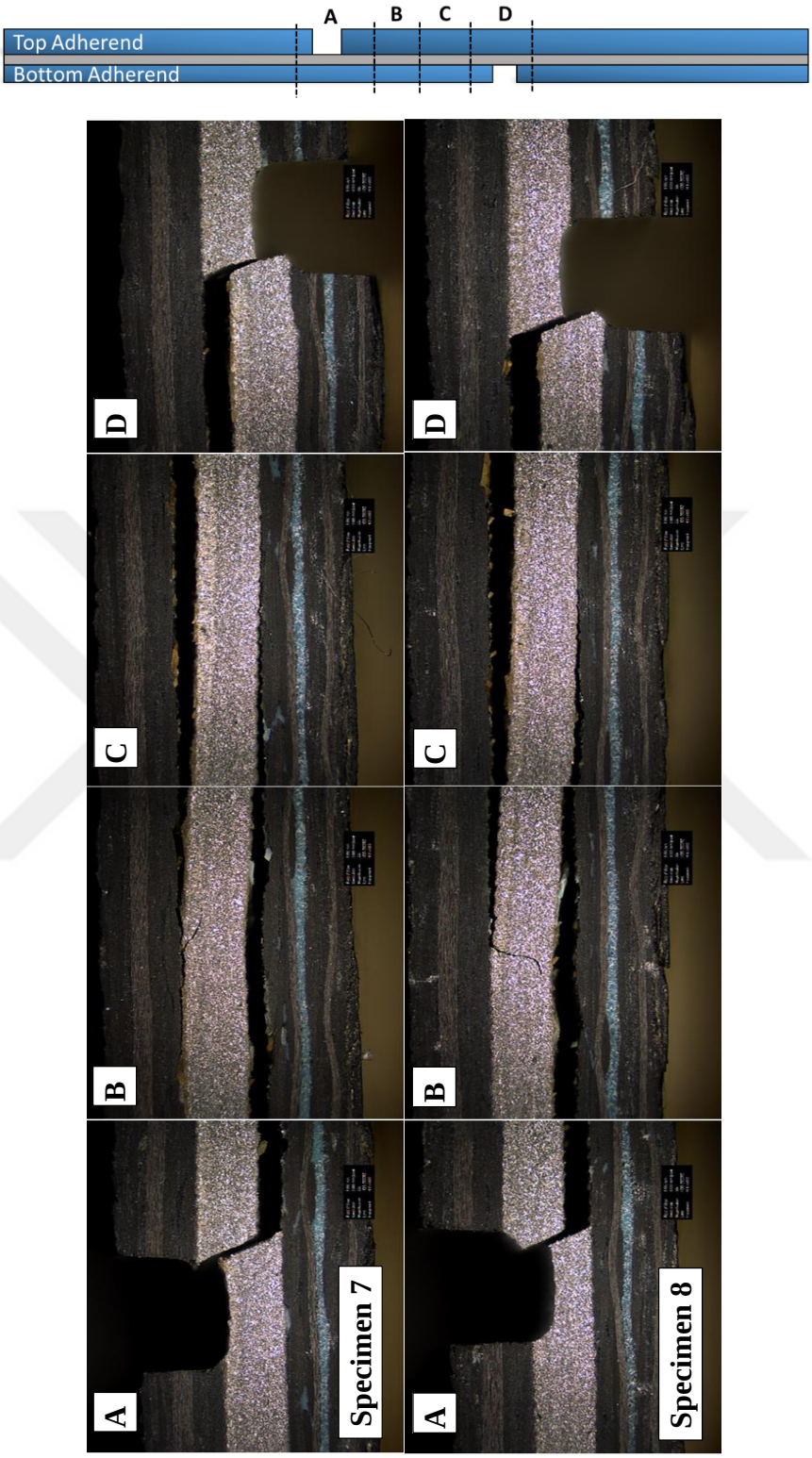

Figure B.4. Microscopic Examination of B5_T10_40 Specimen (Cont.)